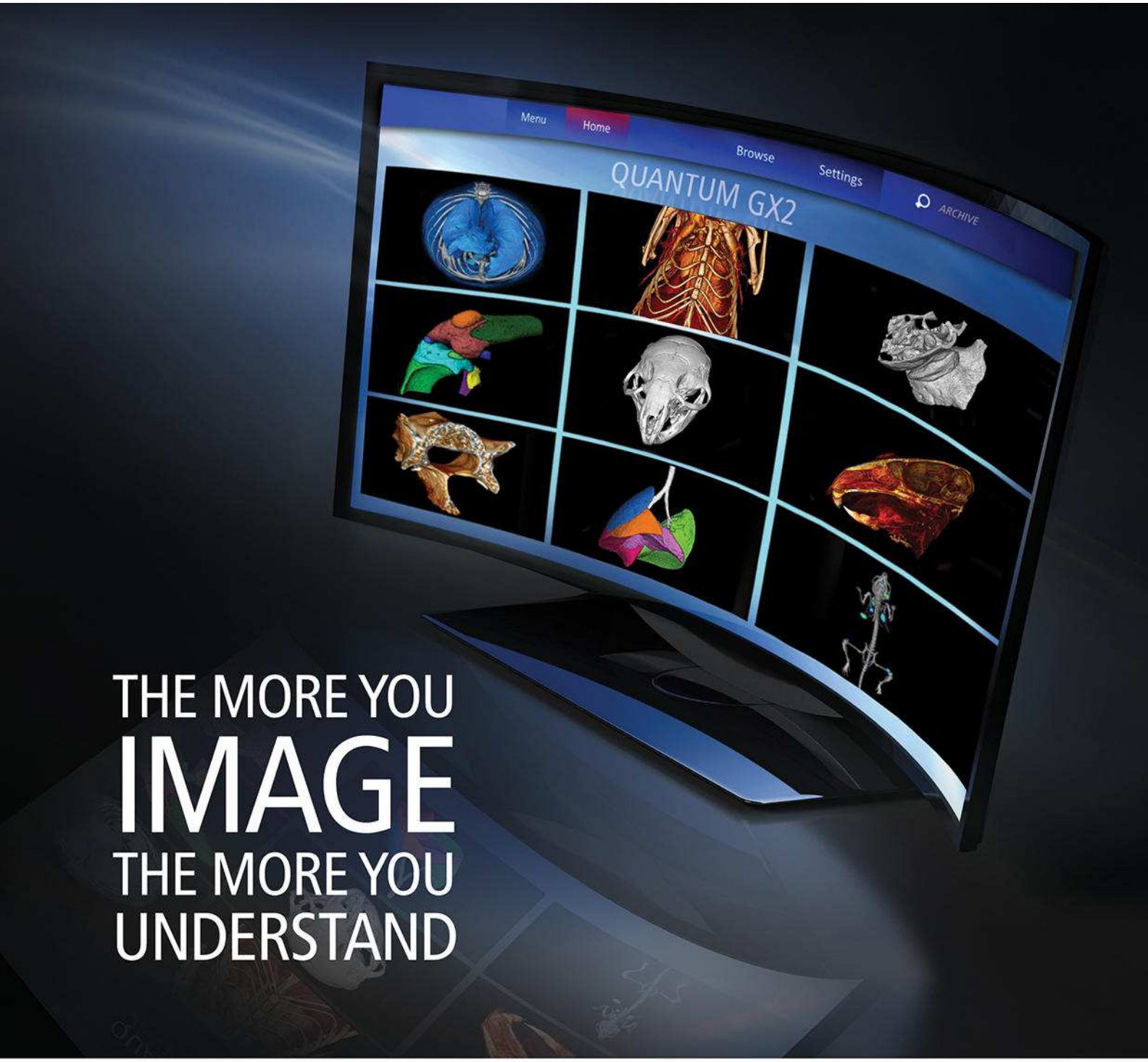

THE MORE YOU IMAGE THE MORE YOU UNDERSTAND

Quantum GX2 microCT

In vivo or *ex vivo*, this is microCT that goes *beyond* bone.

No question, microCT is the go-to modality for bone imaging. But with the Quantum GX2 microCT system, you can image further – investigating cardiovascular, pulmonary, and oncology diseases and beyond. This is a true multispecies scanner – mice, rats, even rabbits can be imaged. It delivers faster scan times and high-resolution *ex vivo* scanning, perfect for longitudinal studies and high-throughput applications. And it can be seamlessly coregistered with our optical platforms to deliver more information on the disease state than microCT alone. With the Quantum GX2, it's not just about imaging, it's about *understanding*.

Learn More

PerkinElmer®
For the Better

ORIGINAL ARTICLE

JBMR®

Osteoblast-Derived Extracellular Vesicles Are Biological Tools for the Delivery of Active Molecules to Bone

Alfredo Cappariello,[1] Alexander Loftus,[1] Maurizio Muraca,[2] Antonio Maurizi,[1] Nadia Rucci,[1] and Anna Teti[1]

[1]Department of Biotechnological and Applied Clinical Sciences, University of L'Aquila, L'Aquila, Italy
[2]Department of Women's and Children's Health, University of Padua, Padua, Italy

ABSTRACT

Extracellular vesicles (EVs) are newly appreciated regulators of tissue homeostasis and a means of intercellular communication. Reports have investigated the role of EVs and their cargoes in cellular regulation and have tried to fine-tune their biotechnological use, but to date very little is known on their function in bone biology. To investigate the relevance of EV-mediated communication between bone cells, we isolated EVs from primary mouse osteoblasts and assessed membrane integrity, size, and structure by transmission electron microscopy (TEM) and fluorescence-activated cell sorting (FACS). EVs actively shuttled loaded fluorochromes to osteoblasts, monocytes, and endothelial cells. Moreover, osteoblast EVs contained mRNAs shared with donor cells. Osteoblasts are known to regulate osteoclastogenesis, osteoclast survival, and osteoclast function by the pro-osteoclastic cytokine, receptor activator of nuclear factor κ-B ligand (Rankl). Osteoblast EVs were enriched in Rankl, which increased after PTH treatment. These EVs were biologically active, supporting osteoclast survival. EVs isolated from *rankl*$^{-/-}$ osteoblasts lost this pro-osteoclastic function, indicating its Rankl-dependence. They integrated ex vivo into murine calvariae, and EV-shuttled fluorochromes were quickly taken up by the bone upon in vivo EV systemic administration. *Rankl*$^{-/-}$ mice lack the osteoclast lineage and are negative for its specific marker tartrate-resistant acid phosphatase (TRAcP). Treatment of *rankl*$^{-/-}$ mice with wild-type osteoblast EVs induced the appearance of TRAcP-positive cells in an EV density-dependent manner. Finally, osteoblast EVs internalized and shuttled anti-osteoclast drugs (zoledronate and dasatinib), inhibiting osteoclast activity in vitro and in vivo. We conclude that osteoblast EVs are involved in intercellular communication between bone cells, contribute to the Rankl pro-osteoclastic effect, and shuttle anti-osteoclast drugs, representing a potential means of targeted therapeutic delivery. © 2017 The Authors. *Journal of Bone and Mineral Research* Published by Wiley Periodicals Inc.

KEY WORDS: EXTRACELLULAR VESICLE; OSTEOBLAST; OSTEOCLAST; RANKL; OSTEOPETROSIS; TARGETED SHUTTLING

Introduction

Extracellular vesicles (EVs) represent a large group of complex membrane structures ranging from 40 nm to 1000 nm in diameter.[1–6] They are phospholipidic bilayers encompassing cellular constituents, classified mainly according to their size and mechanisms of biogenesis.[1,7] EVs generally comprise two different classes: small exosomes, of endocytic origin, and microvesicles, arising by budding from the plasma membrane.

When EVs were first observed, they were considered a product of cellular wasting and nonspecific debris.[2] Nowadays, the biologic meaning of EVs has dramatically changed, switching from a concept of a sophisticated detoxifying system of engulfed/dying cells, now attributed only to apoptotic bodies, to a programmed and regulated means of exchange of biologic information, modulated according to cellular needs and status.[1,3,5,8–13] In this view, the mode of intercellular communication acquires one more paracrine mechanism in addition to cell-to-cell, autocrine, juxtacrine, and systemic communications.

To date, there is evidence revealing that EVs are able to shuttle biologically active molecules, such as proteins, lipids, mRNAs, and microRNAs (miRNAs), by many mechanisms of cellular interaction, including juxtacrine signaling, ligand/receptor interaction, protein shedding, and cargo internalization.[3,7,14] EVs can shuttle both ligands and receptors, thus activating new signaling pathways. Additionally, cell-derived EVs appear capable of transferring essential genetic information from one cell to another.[12,15] Furthermore, they are under intense investigation for biotechnological and clinical applications, because EV cargoes can be manipulated to shuttle exogenous information, delivering molecules and drugs directly to the target cells.[5,8,12,13–22]

Bone is a dynamic tissue hosting finely tuned metabolic processes aimed at guaranteeing the health of the bone tissue itself and that of other organs.[23] To this aim, bone harbors an intricate and strictly synchronized remodeling process in which the bone-forming cells (osteoblasts), the bone-resorbing cells

Received in original form June 14, 2017; revised form October 21, 2017; accepted October 31, 2017. Accepted manuscript online November 1, 2017.
Address correspondence to: Anna Teti, PhD, Department of Biotechnological and Applied Clinical Sciences, Via Vetoio - Coppito 2, 67100, L'Aquila, Italy. E-mail: annamaria.teti@univaq.it
Journal of Bone and Mineral Research, Vol. 33, No. 3, March 2018, pp 517–533
DOI: 10.1002/jbmr.3332

(osteoclasts), and the bone-sensing cells (osteocytes) have an intimate crosstalk, with coordinated and controlled coupling. This relationship induces a tightly regulated influence on the activities and functions of these cells. Since the first pivotal molecule in osteoblast-osteoclast coupling was identified,[24,25] more and more pathways and communication mechanisms between bone cells have been brought to light.

One of the most paradigmatic molecules implicated in the osteoblast-osteoclast crosstalk is the receptor activator of nuclear factor κ-B ligand (Rankl).[25] Rankl is predominantly a transmembrane protein, also occasionally cleaved into a soluble form, which in bone is expressed by osteoblasts and osteocytes and which binds its receptor, Rank, on the surface of osteoclasts and monocytes. The Rankl/Rank axis is a pivotal mediator of osteoclastogenesis, osteoclast function, and osteoclast survival, and both human and murine osteopetrosis forms characterized by the absence of osteoclasts have been demonstrated to carry loss-of-function mutations of these genes.[26]

Based on the complexity of the cellular cycle governing bone remodeling and the exchange of a plethora of molecules between cells in the bone microenvironment, the involvement of EVs in bone pathophysiology is a potential piece of the complex puzzle of bone cellular crosstalk. Despite the dramatic interest in EVs in many fields, their roles in bone biology are still poorly understood. Very few articles have reported the characterization of their molecular profile and activity, and it is possible that the real physiologic role of EVs in the bone microenvironment has been underestimated because only immortalized or tumor cells have been investigated so far, which exhibit intrinsic genetic abnormalities (ie, viral and pro-oncogenic genes).[27–29]

In this study, we focused on mouse primary osteoblast-released EVs and characterized some of their biologic aspects, revealing that they have a previously unrecognized role in the bone cell crosstalk, and demonstrating their relevance as a useful tool to cleverly target bone cells.

Materials and Methods

Animals

Mice were employed for cell cultures and in vivo experiments in conformity with national and international laws and policies (EEC Council Directive 86/609, OJ L 358, Dec. 12, 1987; Italian Legislative Decree, Gu n.61, 14/03/2014) and the NIH Guide for the Care and Use of Laboratory Animals (8th edition. Washington, DC: National Academies Press; 2011). Their use was approved by the Institutional Review Board of the University of L'Aquila, Italy. At the end of the in vivo experiments and for primary cultures, mice were euthanized by CO_2 inhalation. Mice treated with EVs starting at 5 days of life and subjected to blood collection were euthanized by decapitation. For in vivo, ex vivo, and in vitro experiments, wild-type mice were of the CD1 and the C57/BL6 backgrounds, whereas *rankl*$^{-/-}$ (*tnfsf11*$^{-/-}$) mice were of the C57/BL6 background.

Mice were purchased by Charles River-Laboratories Italia S.r.l (Milan, Italy), housed in the animal facility of the University of L'Aquila, Italy, at the following conditions: temperature, 20°C to 24°C; humidity, 60% ± 5%; dark/light cycle, 12/12 hours. They had access to food and water *ad libitum*, and were fed with a normal diet (Mucedola code: #3KE25, Mucedola S.R.L., Settimo Milanese, Italy).

For the in vivo EV kinetics and biological effects, the sample size was calculated using dedicated software (SigmaPlot; Systat Software, Inc., San Jose, CA, USA) based on the expected differences.

Cell cultures

Primary osteoblasts were obtained from skull bones of 7-day-old to 10-day-old CD1 mice (both genders). Calvariae were excised and sequentially digested three times with 1 mg/mL *Clostridium histolyticum* type IV collagenase (Sigma–Aldrich, St. Louis, MO, USA; #C5138-1G) and 0.25% trypsin (Becton Dickinson, Franklin Lakes, NJ, USA) dissolved in Hank's buffered salt solution (HBSS; Gibco, Grand Island, NY, USA). Osteoblasts derived from the second and third digestions were cultured in DMEM containing 10% fetal bovine serum (FBS; Gibco), glutamine (5 mM; Gibco), and penicillin/streptomycin (5 U/mL; Gibco).

For transwell experiments, primary murine osteoblasts (2×10^5 cells/transwell six well) were centrifuged at 400*g* for 5 min and washed twice in PBS. Then, cell suspension was labeled with 1 μM PKH26 (Sigma–Aldrich; #MINI26-1KT) for 5 min and washed twice (5 min × 2) in complete DMEM (10% FBS). A transwell system with a 1-μm pore size membrane (BD Biosciences cell culture insert, Erembodegem, Belgium) was used for culturing PKH26-labeled osteoblasts in the upper chamber and unstained cells in the lower chamber. In both chambers, cells were plated at a density of $1 \times 10^6/cm^2$.

Mature osteoclasts were obtained from bone marrow buffy coat mononuclear cells (BMMs) of 10-day-old CD1 mice (both genders). BMMs were seeded at a density of 1.2×10^6 cells/cm^2 and cultured in DMEM (containing penicillin, streptomycin, and L-glutamine) supplemented with 10% FBS and recombinant human (rh) macrophage colony-stimulating factor (rhM-CSF, 50 ng/mL; PeproTech, Rocky Hill, NJ, USA). After 3 days, osteoclast differentiation was induced by adding rhRankl (120 ng/mL; PeproTech) for an additional 3 days. Mature osteoclasts were then harvested, seeded (1.5×10^5 cells/cm^2), starved in DMEM supplemented with 0.2 mg/mL in bovine serum albumin (BSA; Sigma–Aldrich) for 12 hours and treated with EVs or drugs for 48 hours.

Primary mouse monocytes were obtained as described in the previous paragraph, without the treatment with the rhM-CSF and rhRankl.

EA.hy926 human endothelial cell lines were obtained from the American Tissue Culture Collection (ATCC, Manassas, VA, USA).

EV isolation and staining

EV were isolated from untreated osteoblasts or from osteoblasts treated every 12 hours with 1×10^{-7}M rhParaThyroid Hormone (rhPTH; Sigma–Aldrich).[30] Upon reaching 80% confluence, cells were washed in PBS and starved in serum-free DMEM to prevent FBS EV contamination. After 24 hours, culture medium was harvested and sequentially centrifuged at 4°C at 5,000*g* for 20 min to remove cell debris, 35,000*g* for 20 min to remove apoptotic bodies, and 100,000*g* for 70 min to spin down EVs. The pellets containing EVs were then incubated for 30 min at 37°C with either the membrane-permeant green dye 5-chloromethylfluorescein diacetate (CMFDA) (Thermo Fisher Scientific, Waltham, MA, USA; #C7025) or with the SYTORNA-Select Green Fluorescent Cell Stain (Thermo Fisher Scientific; #S32703), and for 5 min at 37°C with the cell membrane labeling linker PKH26. Then, the EVs were washed in PBS by ultracentrifugation at 100,000*g*, at 4°C for 70 min. Finally, the pelleted EVs were resuspended in a volume of PBS according to the application, and immediately used for the experiments or

stored at –80°C. All cell treatments were performed using EV suspensions derived from 2.5×10^6 cells/cm^2.

Western blot analysis

Osteoblasts and their EVs were lysed in radioimmunoprecipitation assay (RIPA) buffer and protein content was quantified by the bicinchoninic acid (BCA) assay (Thermo Fisher Scientific; #23225). Proteins were separated by SDS-PAGE in nonreducing conditions, and blotted onto nitrocellulose membrane, which was incubated overnight at 4°C with primary CD63 antibody (1:200; BioLegend, San Diego, CA, USA; #143902). After 1 hour incubation at room temperature with horseradish peroxidase (HRP)-goat anti-rat IgG (1:2000) (Santa Cruz Biotechnology, Santa Cruz, CA, USA; Cat. #sc-2006) bands were visualized by Super Signal West Pico chemiluminescent substrate (Thermo Fisher Scientific; #RA227125).

Transmission electron microscopy

For transmission electron microscopy (TEM), 5 μL of EV suspension in PBS was deposited onto Formvar-coated grids and left to air-dry for 20 min. Grids were then washed with PBS and fixed by transfer onto 1% glutaraldehyde for 5 min. After washing with distilled water, samples were contrasted with 4% uranyl-oxalate solution (4% uranyl acetate, 0.15M oxalic acid, pH 7, Sigma–Aldrich–Aldrich) for 5 min. Finally, grids were air-dried for 10 min and observed under a Philips CM 30 TEM at 80 kV.

FACS of EVs

EV pellets were loaded with CMFDA and incubated with a phycoerythrin (PE)-conjugated anti-Rankl antibody (1:100; BD Biosciences; Cat. #560295) for 30 min at 4°C, then CMFDA-loaded, Rankl-positive and Rankl-negative EVs were sorted by FACS. Nanofluorescent standard particles (Spherotech, Lake Forest, IL, USA; cat# NFPPS-52-4K) were used to set dimensional gate up to 1 μm. Routine immunophenotype evaluation was performed on BD FACSCANTO II. Sorting of pure EV population was performed on BD FACSARIA II.

Gene expression

Conditioned media from osteoblasts were processed for EV isolation by ultracentrifugation as described in the "EV isolation and staining" section. Donor osteoblasts were massively washed in PBS (to eliminate any contaminants from the EVs present in the conditioned medium) and trypsinized. Osteoblast suspension was washed twice in PBS by centrifugation at 300*g* for 5 min at 4°C, then 1 million of these cells and the EV pellet were processed for RNA extraction by RNeasy mini kit (Qiagen, Valencia, CA, USA; cat #74104), according to the manufacturer's instructions, and quantified using a NanoDrop 2000 spectrophotometer (Thermo Fisher Scientific).

For large-scale analysis, 32 ng of total RNA were retrotranscribed by PreAMP cDNA Synthesis Primer Mix for mouse Osteoporosis, then the cDNA was ran on a mouse Osteoporosis PCR array (Qiagen; cat#PAMM-170Z).

For semiquantitative RT-PCR of the RNA extracted from EVs, 100 ng of RNA were reverse transcribed using the Moloney murine leukemia virus reverse transcriptase, subjected to PCR reaction that was performed by the DreamTaq Green master mix (Thermo Fisher Scientific) and verified by electrophoresis of PCR products in 2% agarose gel plus ethidium bromide. Primer pairs were as follows: *Gapdh*, forward 5′-TGGCAAAGTGGAGATTGTTGC-3′; reverse 5′-AAGATGGTGATGGGCTTCCCG-3′; *Col-1α1*, forward 5′- GTCCCTCTGGAAATGCTGGAC-3′; reverse 5′-GACCGGGAAGACCGACCA-3′.

For semiquantitative RT-PCR of the RNA extracted from primary osteoblasts treated with PBS (control) or with osteoblast-derived EVs, 1 μg of RNA was retrotranscribed and subjected to PCR as described in the previous paragraph using the following primer pairs: *Gapdh*, forward 5′-TGGCAAAGTGGAGATTGTTGC-3′; reverse 5′-AAGATGGTGATGGGCTTCCCG-3′; *Alp*, forward 5′-CTGGGAG TCTCATCCTGAGC-3′; reverse 5′-CCAGCAGGTTTCTCTGTTGG-3′; *Runx2*, forward 5′-GCCGGGAATGATGAGAACTA-3′; reverse 5′-GGA CCGTCCACTGTCACTTT-3′; *Atf4*, forward 5′-TCGATGCTCTGTTTCGAATG-3′; reverse 5′-AGAATGTAAAGGGGGCAACC-3′; *Osterix*, forward 5′-AGAATCCCTTTCCCTCTCCA-3′; reverse 5′-TGCTTCCCAAT CCTATTTGC-3′; *Col-1α1*, forward 5′- GTCCCTCT GGAAATGCTGGAC-3′; reverse 5′-GACCGGGAAGACCGACCA-3′; *Bglap*, forward 5′-CTTGGGTTCTGACTGGGTGT-3′; reverse 5′-GCCCT CTGCAGGTCATAGAG-3′.

PCR conditions were 94°C for 30 s, 60°C for 30 s, and 72°C for 30 s, replicated for 35 cycles.

EV loading with anti-osteoclast drugs

Sodium zoledronate (Sigma–Aldrich) was dissolved in PBS at a concentration of 14mM, and dasatinib (Selleckchem, Munich, Germany) was dissolved in DMSO at a concentration of 10mM. EVs from 2.5×10^6 osteoblasts/cm^2 were incubated with either drug for 1 hour at 37°C, then they were extensively washed in PBS and ultracentrifuged twice at 100,000*g* for 70 min.

In vitro EV biologic effects

Mature osteoclasts were starved in serum-free DMEM as described in the "Cell cultures" section and treated for 48 hours with EVs (intact or drug-loaded) derived from 2.5×10^6 osteoblasts/cm^2. Osteoclasts were then fixed in paraformaldehyde/PBS (4% vol/vol), cytochemically stained for the osteoclast marker tartrate-resistant acid phosphatase (TRAcP) (Sigma–Aldrich; #387A-1KT) and counterstained with 1μM Hoechst 33342 (Sigma–Aldrich) to identify the nuclei.

Ex vivo EV integration into bone

Seven-day-old CD1 mice were euthanized, their calvariae excised, plated in 35-mm dishes in DMEM with 10% FBS and incubated with PKH26-labeled EVs. After 48 hours, EV integration in the calvarial bones was evaluated by an Olympus Fv1000 confocal microscope (Olympus, Waltham, MA, USA).

In vivo EV kinetics and tissue targeting

Cryopreserved FACS-sorted Rankl-positive and PKH26-labeled EVs were injected intraperitoneally into 5-day-old CD1 male mice. Groups of animals ($n = 6$ each) were euthanized after 1.5, 3, 6, 24, and 48 hours and blood, liver, spleen, kidney, and bones were collected and processed for PKH26 extraction in chloroform-methanol (2:1 vol/vol) and 0.125% sodium dodecyl sulfate. The PKH26 fluorescence intensity was measured by spectrofluorometry (excitation wavelength 550 nm; emission wavelength 567 nm) in the extracted lipid fraction.

In vivo EV biologic effects

Five-day-old C57BL/6 *rankl*$^{-/-}$ male mice were injected intraperitoneally daily for 5 days with 30,000, 60,000, or 120,000

Rankl-positive EVs or with vehicle (PBS) as control. Then, mice were euthanized and tibias excised, fixed for 24 hours in 4% paraformaldehyde, dehydrated with ethanol, and embedded in methoxymethylmetacrylate without decalcification. TRAcP histochemical staining was performed to identify and quantify TRAcP-positive cells belonging to the osteoclast lineage.

Eight-week-old C57BL/6J mice were treated for 4 days with 120 mg/kg body weight (bw) of retinoic acid (Sigma–Aldrich; cat. #R2625, vitamin A acid) administered by oral gavage.[31,32] Mice ($n = 5$/group) were treated once, at day 1 of the experiment, by intraperitoneal injection of vehicles (PBS for sodium zoledronate and 0.1% DMSO for dasatinib), 70 μg/kg bw of sodium zoledronate, 12.5 mg/kg bw of dasatinib, osteoblast EVs loaded with a solution of 14mM sodium zoledronate, osteoblast EVs loaded with a solution of 10 mM dasatinib, or naive osteoblast EVs (2.5×10^6 osteoblasts/cm^2). One group of mice was also sham-treated by oral gavage with the retinoid acid vehicle (corn oil). At the end of the experiment, mice were euthanized. The hind-limb long bones were removed, fixed in 4% paraformaldehyde for methoxymethylmetacrylate embedding without decalcification, histochemically stained for TRAcP activity, and histomorphometrically analyzed for the osteoclast variables according to Dempster and colleagues.[33] Counterstaining with hematoxylin was performed to evaluate osteoclast apoptosis.

For the in vivo experiments, three to six mice were employed per each group of treatment, allocated after randomization in number of three mice/cage. Treatments and measurements were performed in blind. No adverse effects were observed following treatment with EVs.

Statistics

Data were reported as mean ± standard deviation (SD). Student's t test between two groups or one-way ANOVA using nonparametric Kruskal-Wallis test between multiple groups were used as comparative statistical methods, with a significant p value <0.05 (GraphPad Prism 7.00; GraphPad Software, Inc., La Jolla, CA, USA). All in vitro experiments were performed with three technical replicates for each point and repeated at least three times or using three to six mice/group.

Results

Osteoblasts release membrane-derived structures into their surroundings

To investigate whether physiologic cell-to-cell communication in bone cells could involve EVs, we focused on osteoblasts, the active matrix-forming cell type in the bone, examining clues of intercellular communication based on EV exchange. Primary murine osteoblasts, labeled with the red fluorescent cell membrane dye PKH26, were plated in the upper chamber of 1-μm pore transwell dishes, allowing the passage of EV-sized particles, while unstained osteoblasts were plated in the lower chamber (Fig. 1*A*). The cultures were monitored and after 48 hours we observed the appearance of red fluorescence in the previously unstained osteoblasts in the bottom chamber (Fig. 1*B*), indicating the fusion of donor cell–labeled plasma membrane derivatives as well as their integration in the target cells.

EVs are harvestable from osteoblast conditioned media

To confirm the involvement of EVs in the transfer of membrane-bound dyes, we analyzed the release of EVs from cultured osteoblasts. We collected 24-hour serum-free conditioned media from primary mouse calvarial osteoblasts. After ultracentrifugation, the pellets were assessed for protein content (Fig. 1*C*, left bar). To further evaluate at the molecular level whether or not our ultracentrifugation pellet contained EVs, we performed a Western blot for the commonly-reported exosome marker CD63.[3] The enrichment of CD63 in our ultracentrifugation pellets compared to the total cell lysates indicated the isolation of a concentrated population of EVs (Fig. 1*D*). The same evaluation performed in cryopreserved EVs demonstrated that this marker was not lost upon freezing (Fig. 1*D*).

To confirm the presence of intact EVs obtained by ultracentrifugation, we loaded the EVs of the isolated pellets with the membrane-permeant fluorescent probe CMFDA. This dye is cleaved intracellularly by cytosolic esterases into a non-permeant molecule that does not leak out from intact membranes. By fluorescence microscopy, we observed in the pellets a population of green-fluorescent apparently integral vesicular structures (Fig. 1*E*). Finally, a deeper morphologic evaluation by TEM analysis showed the expected heterogeneous population of intact and spheroid membrane bodies (Fig. 1*F*), which matched the expected size distributions of EV populations.[1]

Next, we questioned whether EV release was a physiologically controlled process. Because it has been reported that cells can respond to stimuli by increasing vesiculation,[34] we treated osteoblast cultures with 1×10^{-7}M rhPTH, a potent regulator of osteoblast activity.[30] Although the donor osteoblast cell protein content was not affected by PTH (untreated osteoblasts, 1.1 ± 0.13 mg; PTH-treated osteoblasts, 1.05 ± 0.02 mg; $p = 0.6$), the protein content of the EV pellet obtained from the conditioned media of PTH-treated osteoblasts was higher than from control conditioned media (Fig. 1*C*, right bar), supporting the hypothesis that this release was a hormonally regulated process.

Finally, we investigated whether EVs were able to target cells and transfer fluorophores. We incubated the CMFDA-loaded EVs with primary murine osteoblasts and monocytes, two of the most abundant cell types in bone and bone marrow, respectively, confirming the integration of this fluorescent probe in both recipient cells (Fig. 1*G*,*H*).

Qualitative and quantitative analysis of osteoblast-derived EVs by FACS

To confirm the cellular origin and integrity of the membrane structures, we next performed a FACS analysis after incubation of EV pellets with CMFDA. We noted that 16.67% ± 1.93% of events analyzed in the ultracentrifugation pellet represented CMFDA-positive structures up to 1 μm in diameter, consistent with the size of EVs (Fig. 1*I*,*J*). Given that CMFDA is a dye that does not leak out from integral membrane particles, we concluded that these structures were intact. The CMFDA-positive particles were sorted and their morphology was evaluated by TEM, confirming the expected EV size distribution and apparent membrane integrity (Fig. 1*K*).

We next assessed whether FACS-sorted EVs retained the ability to fuse with target cells. To this aim, we incubated primary osteoblasts with FACS-sorted CMFDA-loaded PKH26-labeled EVs. Microscopic analysis showed the integration of both fluorophores into target cells (Fig. 2*A*, left panels). Trypsin/EDTA treatment of target cells did not compromise the presence of the dyes in their cytoplasm (Fig. 2*A*, right panels), confirming

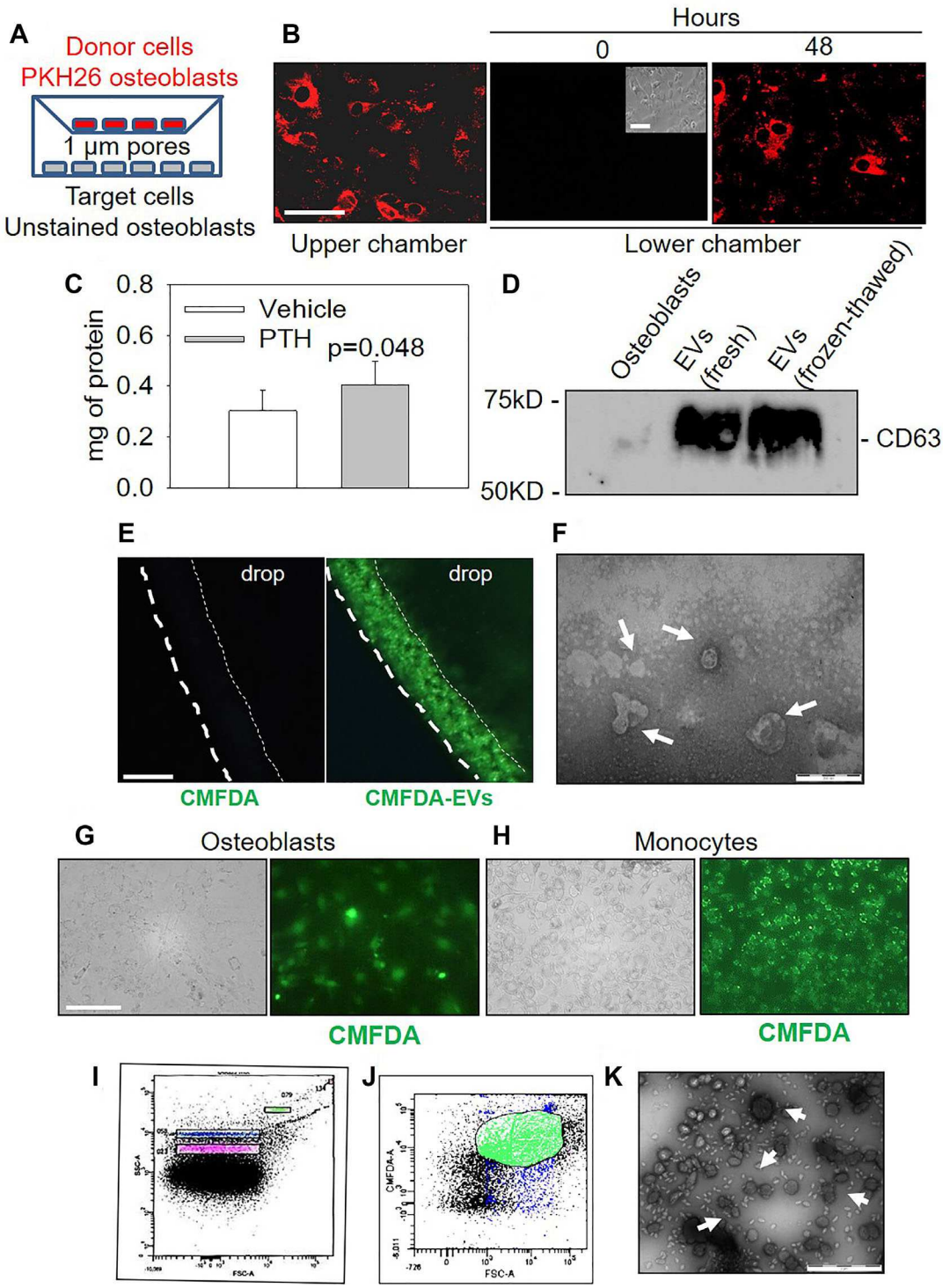

Fig. 1. Characterization of osteoblast EVs. (*A*) Cartoon illustrating the experiment performed in transwell. (*B*) PKH26-labeled donor osteoblasts (left panel), unlabeled target osteoblasts at time 0 (inset phase contrast) (middle panel), and previously unlabeled osteoblasts after 48 hours of incubation in transwell with the PKH26-labeled osteoblasts (right panel). Scale bar = 5 μm. (*C*) Protein titration of EVs isolated by ultracentrifugation from serum-free media of vehicle-treated or PTH (1×10^{-7}M)-treated osteoblasts. (*D*) Western blot for CD63 of osteoblast cell lysate, freshly isolated EVs or frozen-thawed EV lysate from osteoblasts. (*E*) Fluorescence microscopy evaluation of a drop of control free CMFDA (left panel), and EV loaded with CMFDA (right panel). Scale bar = 1 μm. Dotted line, drop edge. (*F*) Morphology of isolated osteoblast EVs (arrows) fixed, contrasted with uranyl-oxalate solution and observed by TEM. Scale bar = 1 μm. Phase contrast (left panels) and fluorescence microscopy (right panels) of (*G*) primary murine osteoblasts and (*H*) monocytes incubated for 48 hours with CMFDA-loaded osteoblast EVs. Scale bar = 5 μm. (*I*) FACS setting for dimensional gate with commercial standard microbeads (purple: 0.23 μm; blue: 0.58 μm; green: 0.79 μm; red: 1.3 μm; Spherotech). (*J*) Dot plot of FACS-analyzed EV pellet isolated by ultracentrifugation from osteoblast conditioned media and loaded with CMFDA. (*K*) Ultrastructure of FACS-sorted CMFDA-loaded osteoblast EVs (arrows) observed by TEM. Scale bar = 1 μm. Results are representative (*B*,*D*–*K*) or the mean ± SD (*C*) of at least three independent experiments (Student's *t* test).

the complete integration of the fluorophores into their intracellular compartment.

Osteoblast-derived EVs target and integrate into recipient cells

We next investigated the kinetics of EV integration into target cells. To this aim, we performed a time-course experiment using osteoblasts incubated with FACS-sorted EVs loaded with CMFDA and labeled with PKH26. By confocal microscopy, we observed a time-dependent integration of EV fluorescent components in target cells starting after 24 hours from EV administration and persisting until at least 48 hours (Fig. 2*B*). The analysis of the integrated dyes showed a typical vesicular distribution. Furthermore, *z*-axis evaluation enabled us to distinguish also domains of the target cells enriched only in one of the two fluorophores with no colocalization in the same areas (Fig. 2*B*). This observation suggests that target cells could process the individual constituents of EVs separately, transferring them to different cellular compartments.

Finally, we investigated the integration of FACS-sorted EVs with other cell types, such as endothelial cells and monocytes, with which the osteoblasts exchange important molecular information. Fluorescence microscopy confirmed that both human umbilical vein cell line EA.hy926 and primary mouse monocytes internalized the fluorochromes shuttled by EVs (Fig. 2*C*), suggesting also a mouse-human cross-species integration.

Osteoblast-derived EVs contain Rankl

Because EVs are reported to trigger ligand/receptor interactions in target cells,[16,17] we asked whether EVs from osteoblasts

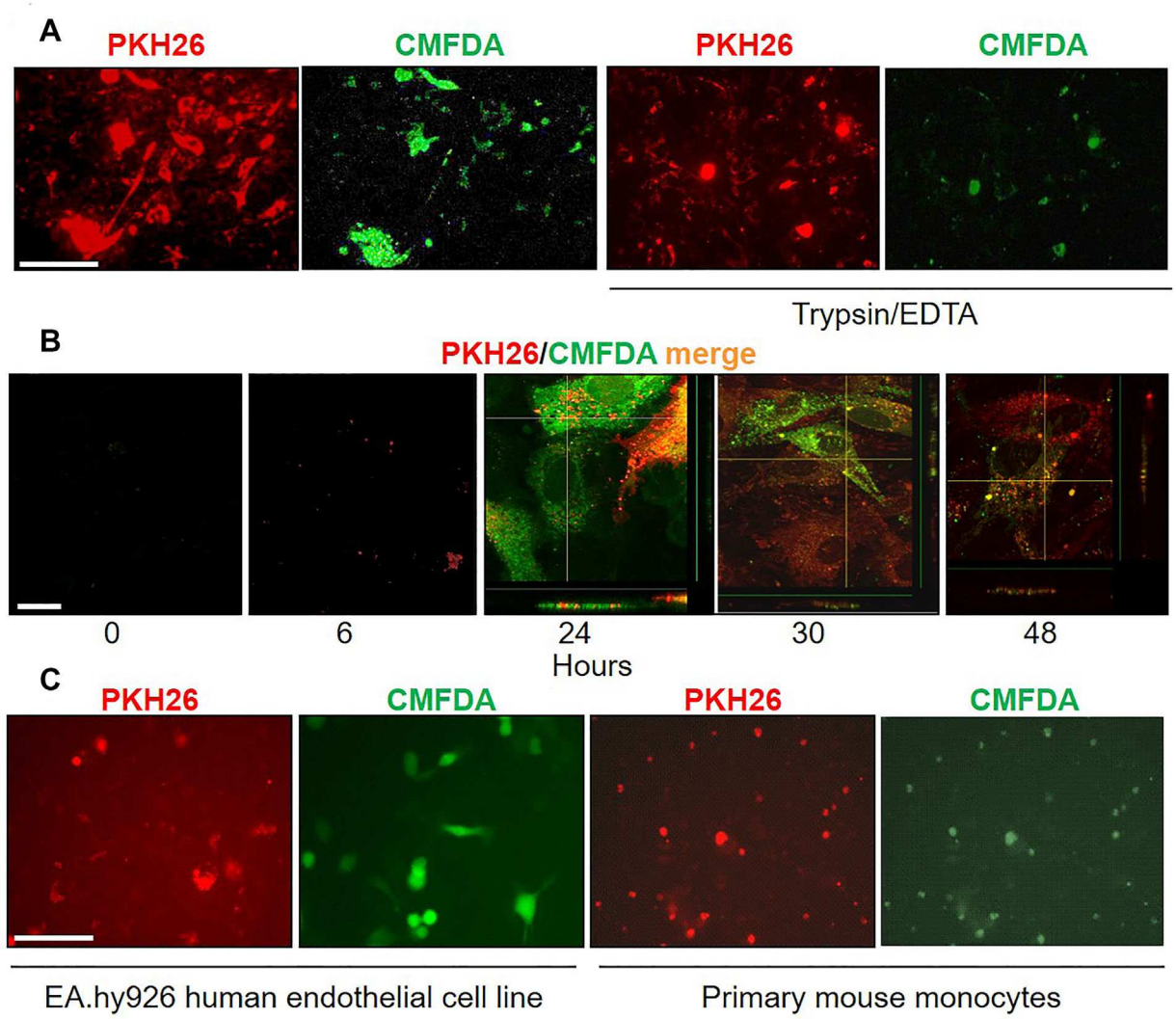

Fig. 2. Osteoblast EV integration in target cells. (*A*) Evaluation by conventional epifluorescence microscopy of osteoblasts incubated for 2 days with osteoblast EVs previously labeled with PKH26 (red) and CMFDA (green) fluorescent dyes. Integration of the dyes in target cells before (left panels) and after (right panels) trypsin-EDTA treatment. Scale bar = 20 μm. (*B*) Confocal microscopy analyzing a time course experiment of osteoblasts incubated for 2 days with FACS-sorted osteoblast EVs labeled with PKH26. Scale bar = 5 μm. (*C*) Evaluation by conventional epifluorescence microscopy of endothelial cell line and primary murine monocytes incubated up to 48 hours with osteoblast EVs previously labeled with PKH26 (red) and CMFDA (green) fluorescent dyes, which were integrated in target cells. Scale bar = 20 μm. Results are representative of three independent experiments.

could shuttle Rankl, one of the most important intercellular crosstalk molecules in bone. We therefore investigated the presence of membrane-bound Rankl by FACS in osteoblast EVs and observed that 53.95% ± 3.48% of them were Rankl-positive (Fig. 3*A*). To further characterize the quality of FACS-sorted EV preparations, we performed TEM analysis of Rankl/CMFDA-double positive EVs and observed a heterogeneous population of intact spheroid bodies, with the expected EV morphology and size distribution (Fig. 3*B*).

Because we noted that PTH increased EV production by osteoblasts (Fig. 1*C*), and given that PTH is a well-known inducer of Rankl expression,[30] we evaluated the proportion of osteoblast-derived EVs which were Rankl-positive following treatment with 1×10^{-7}M rhPTH. FACS analysis showed that PTH increased

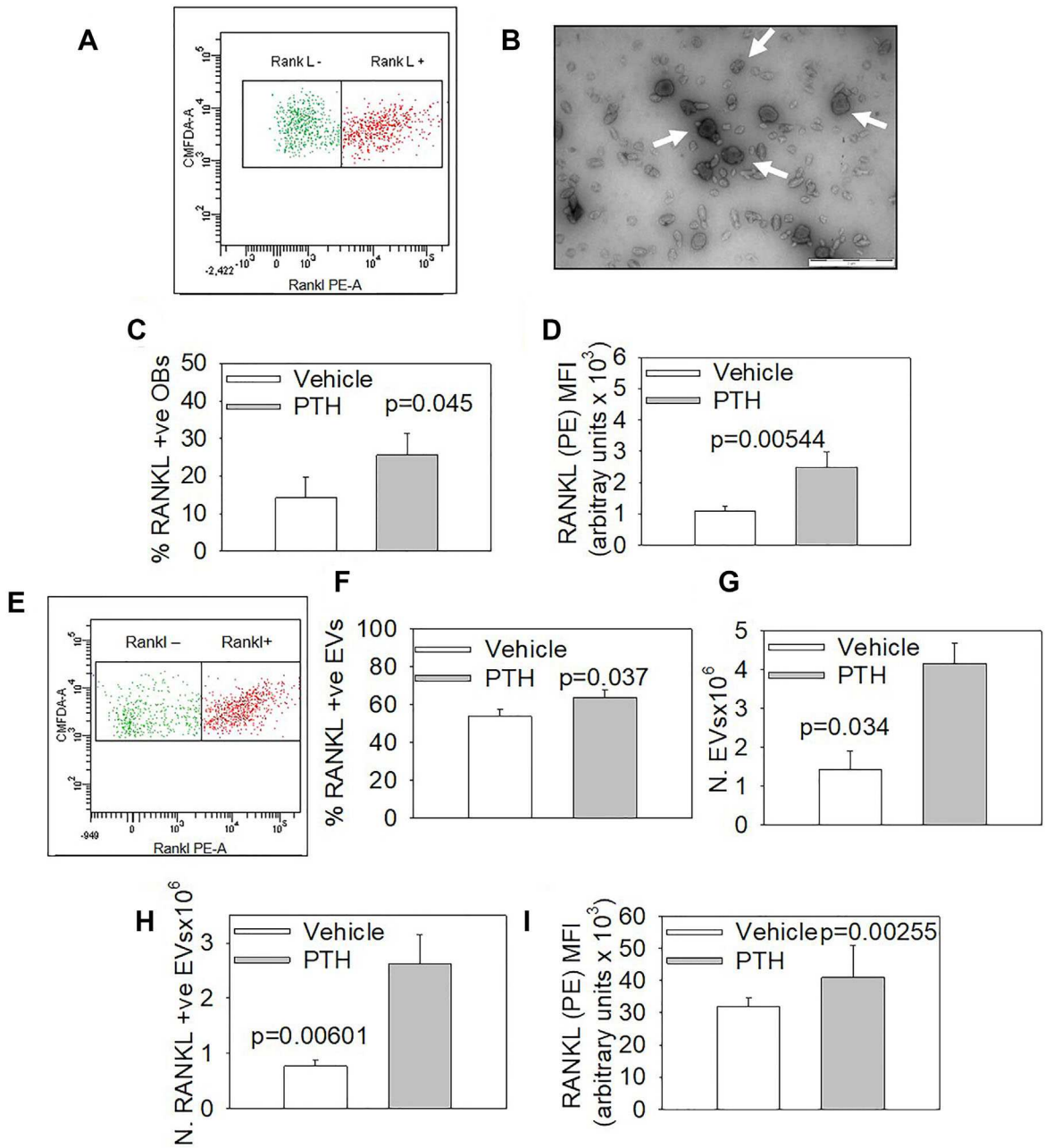

Fig. 3. Analysis of RANKL expression in osteoblast EVs. (*A*) FACS analysis of CMFDA-loaded, PE-Rankl–negative (left gate) and PE-Rankl–positive (right gate) EV populations isolated from primary osteoblast cultures. (*B*) Analysis by TEM of FACS-sorted Rankl-positive osteoblast EVs (arrows). Scale bar = 2 μm. (*C*) FACS quantification of the percentage of Rankl-positive osteoblasts and (*D*) mean (PE)-fluorescent intensity (MFI) per event in primary osteoblast cultures treated with vehicle or PTH. (*E*) FACS analysis of CMFDA-loaded, PE-Rankl–negative (left gate) and PE-Rankl–positive (right gate) EV populations isolated from primary osteoblast cultures treated with vehicle or PTH. (*F–I*) FACS quantification of (*F*) the percentage of Rankl-positive EVs, (*G*) the total number of EVs, (*H*) the number of Rankl-positive EVs and (*I*) the Rankl (PE)-positive MFI per event in EVs isolated from vehicle-treated and PTH-treated osteoblasts. Results are representative (*A*,*B*,*E*) or the mean ± SD (*C*,*D*,*F–I*) of at least three independent experiments (Student's *t* test). OB = osteoblast.

the percent of Rankl-expressing osteoblasts as well as the mean PE-fluorescent units per osteoblast (Fig. 3*C*,*D*). Furthermore, the percentage of RANK-L–positive events increased up to 63.6% ± 4.20% of EVs in PTH-treated ultracentrifugation pellets versus vehicle-treated osteoblasts (Fig. 3*E*,*F*). Consistently, PTH also increased the total number of EVs (Fig. 3*G*), the number of Rankl-positive EVs (Fig. 3*F*), the mean PE-fluorescent units per event (Fig. 3*H*), and the percentage of Rankl-positive events (Fig. 3*I*).

Biologic effects of osteoblast EVs

To assess the biologic effect of EVs on bone cells we investigated the phenotype of osteoblasts and osteoclasts exposed to osteoblast EVs. Semiquantitative RT-PCR performed on control osteoblasts and osteoblasts treated for 48 hours with osteoblast EVs showed no modulation of *Alp*, *Runx2*, and *Atf4*, while osteoblast EVs significantly reduced *osterix* mRNA (Fig. 4*A*,*B*). Likewise, the transcriptional expression of the matrix protein, *Col1α1* was not affected by osteoblast EVs, while *Osteocalcin* was significantly increased compared to control osteoblasts (Fig. 4*A*, *B*). These data suggest selective regulation of osteoblast genes by means of their own EVs.

Next, we evaluated the biologic effect of EVs on osteoclasts and noted that treatment with osteoblast-derived EVs improved osteoclastic variables, increasing osteoclast size and number of nuclei/cell (Fig. 5*A*,*B*). Moreover, the EV-treated osteoclasts stained more strongly for TRAcP than vehicle-treated osteoclasts (Fig. 5*A*). Taken together, these data confirmed a direct biologic effect of osteoblast-derived EVs in cells of the bone microenvironment and supported the concept that EVs are a means of Rankl mediated osteoblast/osteoclast crosstalk.

To establish the involvement of Rankl in the pro-osteoclastic effect of osteoblast-derived EVs, we took advantage of the *rankl*$^{-/-}$ mouse to isolate primary osteoblasts and collect *rankl*$^{-/-}$ EVs. We treated 12-hour-starved osteoclasts for 48 hours with wild-type or *rankl*$^{-/-}$ EVs, noting that *rankl*$^{-/-}$ EVs were less efficient than wild-type EVs in supporting osteoclast survival (Fig. 5*C*–*E*). In fact, osteoclasts treated with *rankl*$^{-/-}$ EVs generally contained fewer nuclei and exhibited signs of nuclear degeneration (Fig. 5*C*–*E*). Moreover, we noted a higher percentage of retracted or disaggregated osteoclasts (Fig. 5*C*–*E*), reminiscent of apoptotic cells. EV retrieval from wild-type and *rankl*$^{-/-}$ osteoblasts was similar, as shown by the protein quantification of the EV pellets from the two genotypes (Fig. 5*F*), ruling out that the observed differences were due to altered EV release by *rankl*$^{-/-}$ osteoblasts. These results demonstrated that EVs can exert a direct effect on osteoclast survival through their Rankl cargo.

EVs are biotechnological tools to shuttle drugs to osteoclasts

EVs have raised great interest as drug carriers.[35] Because we found a clear effect of naïve osteoblast EVs on osteoclasts, we investigated whether they could be manipulated to shuttle anti-osteoclastic agents to target cells. To test this concept, we loaded osteoblast EVs with the clinically-approved anti-osteoclast drugs, sodium zoledronate (N-bisphosphonate) and the tyrosine kinase inhibitor dasatinib. We treated mature osteoclasts for 48 hours with EVs loaded with zoledronate (Fig. 6*A*) (EV-Zol) or dasatinib (EV-Das) (Fig. 6*B*), which induced cell death with high efficiency (Fig. 6*C*,*D*).

Osteoblast-derived EVs shuttle RNAs to recipient cells

EVs are reported to be involved in cell reprogramming via the shuttling of RNAs,[5,10,36] so we examined whether osteoblast-derived EVs contained RNAs. To address this issue, we stained EV

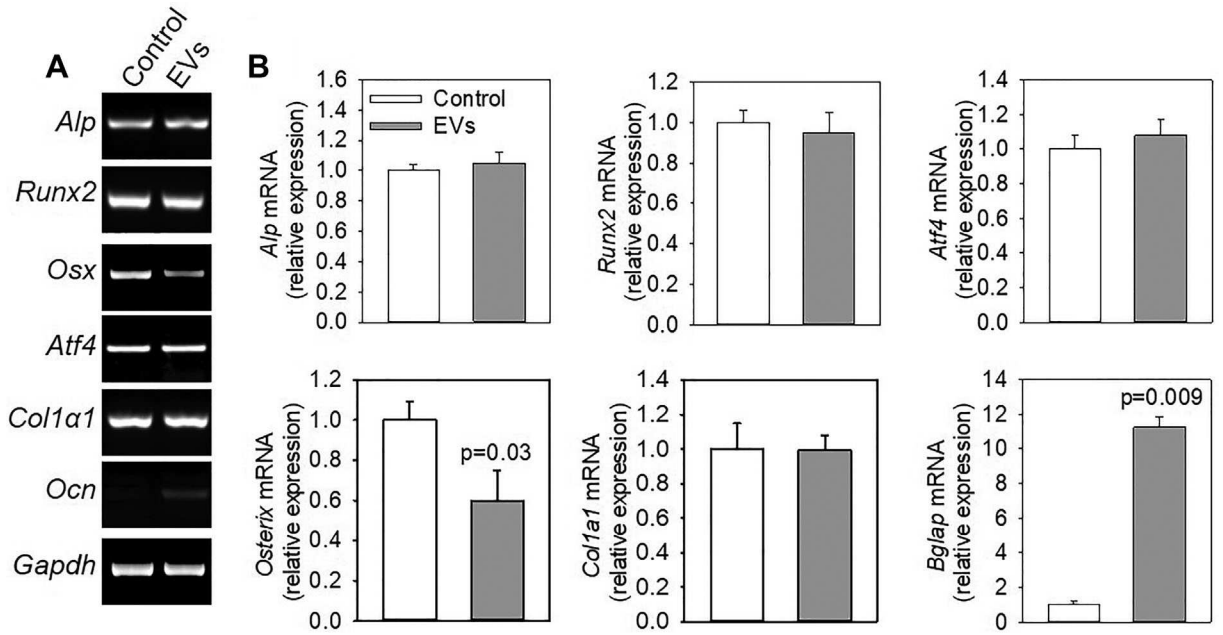

Fig. 4. Autocrine effect of osteoblast EVs on osteoblast gene expression. (*A*) Transcriptional profile of mouse primary osteoblasts treated with PBS (control) or with osteoblast-derived EVs (EVs) by semiquantitative RT-PCR. (*B*) Densitometric analyses of the amplification bands of the indicated genes normalized by the housekeeping gene *Gapdh*. Data are representative (*A*) or the mean ± SD (*B*) of three independent experiments. (Student's *t* test).

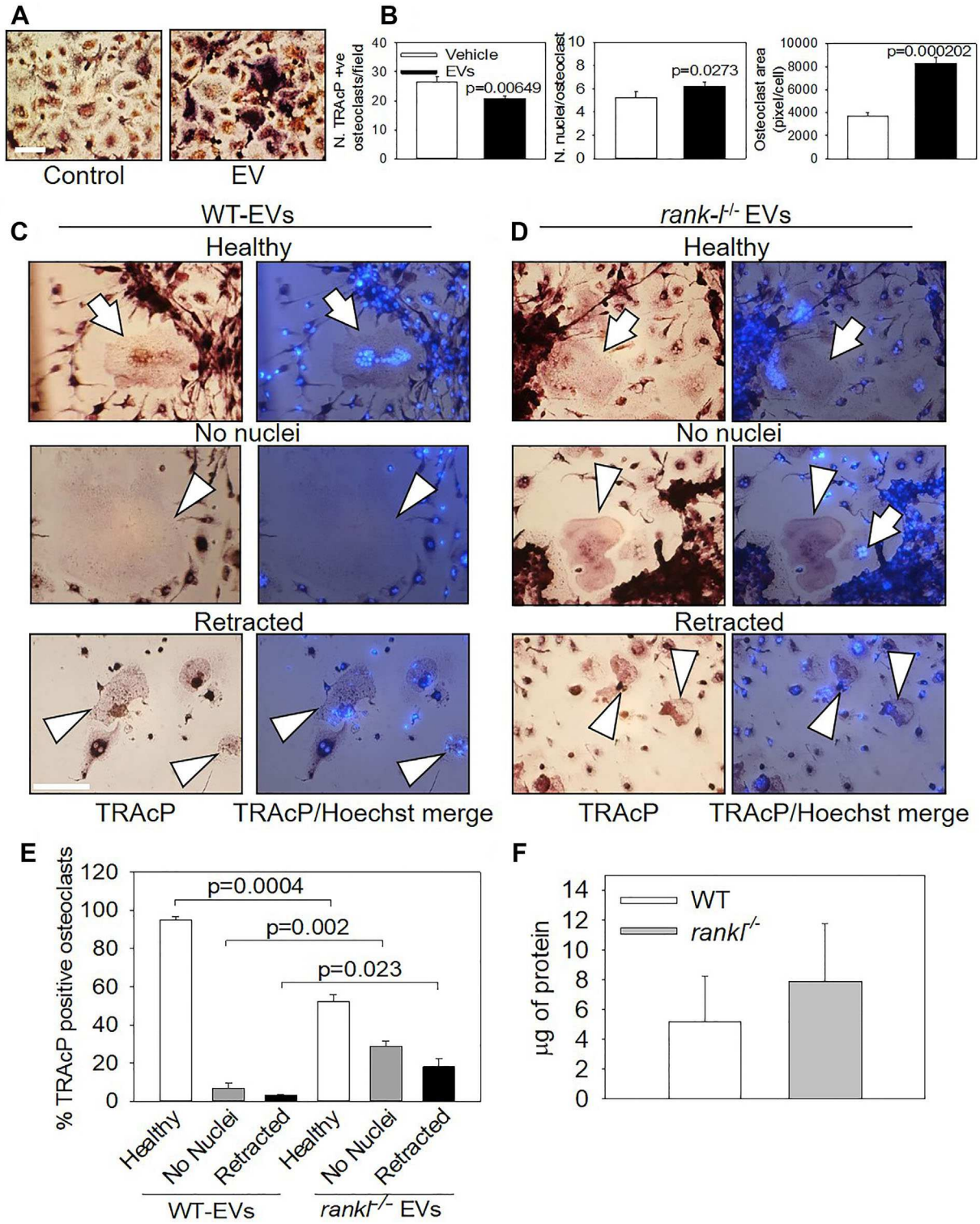

Fig. 5. Effect of osteoblast EVs on osteoclast survival. (*A*) Cytochemical evaluation of TRAcP activity in primary murine mature osteoclasts treated with vehicle or osteoblast-EVs. Scale bar = 5 µm. (*B*) Number of TRAcP-positive multinucleated osteoclasts (left panel), osteoclast area (middle panel), and number of nuclei/osteoclast in vehicle-treated (PBS) or osteoblast EV-treated osteoclast cultures. Microscopic evaluation of mature osteoclasts treated for 48 hours with EVs from (*C*) WT or (*D*) *rankl*$^{-/-}$ osteoblasts. Left panels, TRAcP cytochemical staining of osteoclasts; right panels, Hoechst staining of nuclei. Arrows, healthy osteoclasts; large arrowheads, osteoclasts with no nuclei (ghost cells); small arrowheads, retracted osteoclasts. (*E*) Quantification of the morphological features shown in *C* and *D*. (*F*) Protein titration of EVs isolated by ultracentrifugation from serum-free conditioned media of WT or *rankl*$^{-/-}$ osteoblasts. Results are representative (*A*,*C*,*D*) or the mean ± SD (*B*,*E*,*F*) of at least three independent experiments (Student's *t* test). WT = wild-type.

pellets with SYTO RNASelect, a cell-permeant dye that exhibits bright green fluorescence only when bound to single-stranded nucleic acids. We then treated both primary osteoblasts and monocytes with SYTO-stained EVs, noting the integration of green fluorescence into target cells, thus indicating the shuttling of RNAs (Fig. 7*A*,*B*). FACS analysis revealed that most EVs (97.1% ± 0.26%) were SYTO-positive and contained RNAs (Fig. 7*C*,*D*). Treatment of primary osteoblasts with SYTO-positive FACS-sorted EVs confirmed that green-stained RNAs were transferred into target cells (Fig. 7*E*).

With this data in hand, we characterized the mRNA content of EVs. To achieve this goal we focused on a panel of 84 genes, known to be involved in osteoblast/bone physiology, using a Real-Time Profiler PCR array. We found that EVs from osteoblasts were enriched especially in *Col1a1*, *Col1a2*, *Sparc*, and *Spp1* genes, typically involved in osteoblast function and bone formation (Table 1, Fig. 7*F*). We confirmed the expression of the most abundant gene, *Col1a1*, normalized versus *Gapdh*, by RT-PCR (Fig. 7*G*). A further bioinformatics comparison of transcriptome profile between donor osteoblasts and released EVs showed no significant differences between them (Fig. 7*H*), suggesting that in our conditions the EV transcriptome mirrors the osteoblastic transcriptomic profile.

Osteoblast-derived EVs show marked ex vivo osteotropism and in vivo bone biodistribution

We next investigated whether osteoblast-derived EVs were able to integrate into the bone tissue. To this aim, we incubated mouse calvariae ex vivo with PKH26-labeled osteoblast EVs for 48 hours. Confocal microscopy showed

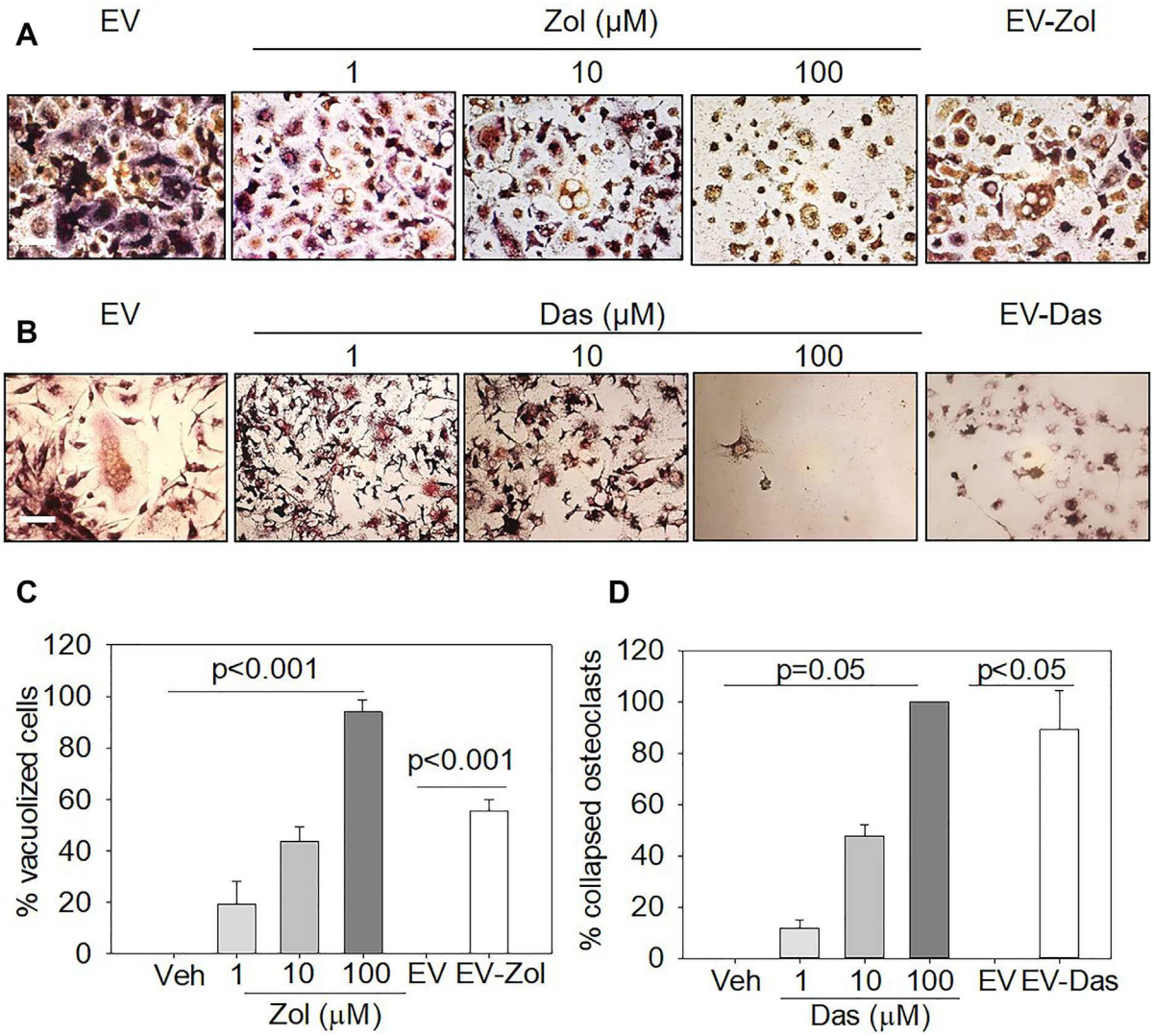

Fig. 6. EVs as drug delivery system. (*A*) Cytochemical evaluation of TRAcP activity in mature primary murine osteoclasts incubated with osteoblast EVs, free Zol (1 to 100μM) or EV-Zol. (*B*) Cytochemical evaluation of TRAcP activity in mature primary murine osteoclasts incubated with osteoblast EVs, free Das (1 to 100μM) or EV-Das. Scale bar = 5 μm. (*C*) Quantification of the features shown in *A*. (*D*) Quantification of the features shown in *B*. Results are representative (*A*,*B*) or the mean ± SD (*C*,*D*) of at least three independent experiments (one-way ANOVA). Zol = zoledronate; EV-Zol = Zol-loaded osteoblast EVs; Das = dasatinib; EV-Das = Das-loaded osteoblast EVs.

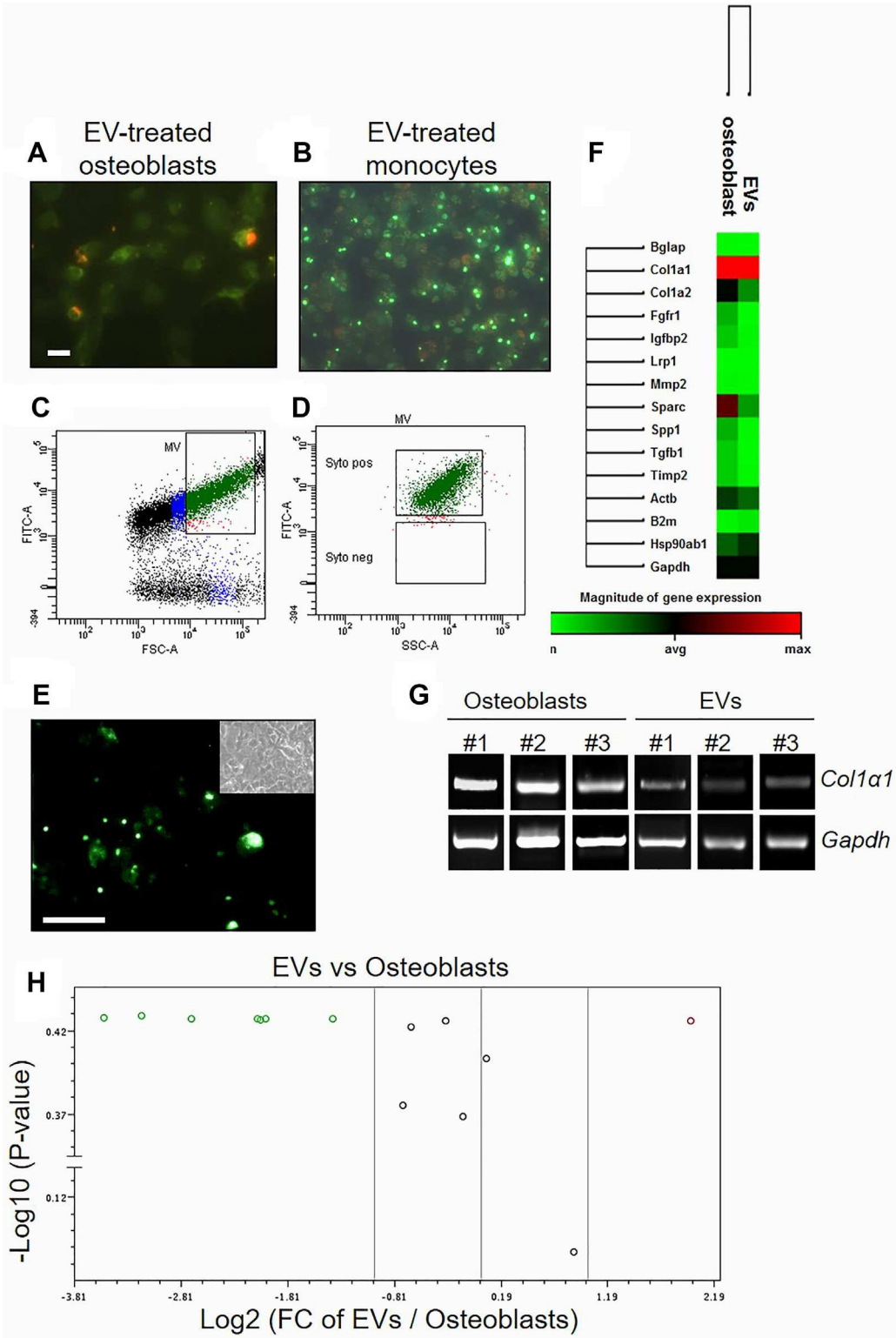

Fig. 7. Characterization of osteoblast EV RNA cargo. Microscopic evaluation of (*A*) osteoblasts and (*B*) monocytes treated for 36 hours with EVs loaded with the RNA-specific green fluorescent dye, SytoRNA Select (unbound dye appears red). Scale bar = 5 μm. (*C*) FACS dot plot of sorted SytoRNA select-stained EVs. (*D*) FACS dot plot of the SytoRNA select-positive and SytoRNA select-negative osteoblast EV population shown in *C*. (*E*) Primary osteoblasts incubated for 36 hours with EVs sorted in *D*. Scale bar = 5 μm. (*F*) Heat map (green = low expressed gene, red = high expressed gene) of genes evaluated on mRNA extracted from osteoblasts and osteoblast EVs by Real-Time Profiler PCR array. (*G*) RT-PCR of mRNA from osteoblasts and osteoblast EVs for the most highly expressed genes identified in *F*. (*H*) Volcano plot assessing the statistical significance (*p* value) depending on FC expression between the osteoblast and osteoblast EV genes listed in *F*. Results are representative (*A*–*G*) or the *p* value (*H*) of three independent experiments (Student's *t* test). FC = fold change.

Table 1. List of the 15 Most Abundant Genes (Cutoff ≤27) Evaluated by Real-Time Profiler PCR Array on mRNA Extract From Osteoblast EVs ($n = 3$)

Rank order	Gene symbol	Cutoff average	SD
1	*Col1a1*	20.62	1.32
2	*Hsp90ab1*	21.88	0.40
3	*Gapdh*	22.08	0.41
4	*Actb*	22.29	0.50
5	*Col1a2*	22.72	0.89
6	*Sparc*	22.89	0.44
7	*B2m*	24.77	1.04
8	*Igfbp2*	25.55	0.55
9	*Timp2*	25.66	0.57
10	*Spp1*	25.72	0.50
11	*Mmp2*	25.77	0.93
12	*Fgfr1*	26.54	0.28
13	*Tgfb1*	26.78	0.05
14	*Bglap*	26.8	0.45
15	*Lrp1*	26.84	0.21

integration of PKH26 into the inner part of the bone (Fig. 8*A*, *B*), supporting the hypothesis of an intrinsic osteotropism and integration of osteoblast EVs. It is known that peritoneal vessel allow EVs to pass into the circulation and reach target organs.[37,38] Therefore, in order to demonstrate that EVs could target the bone tissue in vivo, we performed intraperitoneal injections of 30,000 FACS-sorted Rankl positive EVs, labeled with PKH26, into 5-day-old CD1 pups. Kinetic evaluation of PKH26 distribution in tissues revealed a fast uptake of PKH26 in bones, which peaked at 1.5 hours from EV injection, declining thereafter to a plateau within 24 hours (Fig. 8*C*). PKH26 fluorescence was also observed in blood cells, liver, spleen and kidney, but with lesser intensity or slower kinetics (Fig. 8*C*). In liver, a peak of PKH26 fluorescence was observed after 24 hours from EV injection (Fig. 8*C*), suggesting clearance of the dye from the other tissues. Confocal microscopy on optimal cutting temperature (OCT)-embedded liver sections showed the presence of PKH26 spots (Fig. 8*D*,*E*), confirming the accumulation of PKH26 in the liver parenchyma.

Osteoblast-derived EVs shuttle specific information to bone in vivo

To further investigate the effect of EVs on bone physiology, we focused on the osteoclast lineage and performed in vivo experiments in *rankl*$^{-/-}$ mice, a murine model of severe osteopetrosis characterized by the lack of osteoclasts and the consequent absence of the osteoclast biomarker TRAcP in the bone. We intraperitoneally injected increasing amounts of FACS-sorted Rankl-positive osteoblast EVs into *rankl*$^{-/-}$ mice. Histochemical analysis of tibial sections revealed the presence of TRAcP-positive cells in all EV treatments. In contrast, TRAcP positivity was totally absent in vehicle-injected mice (Fig. 8*F*–*K*). The total number of TRAcP-positive cells did not vary between the EV treatment regimens (Fig. 8*J*), but the total TRAcP-positive area increased with the number of injected EVs (Fig. 8*K*). These results suggest that Rankl-positive EVs exhibit a direct in vivo osteoclastogenic potential.

Osteoblast EV-encapsulated drugs inhibit osteoclast activity in vivo

To investigate whether osteoblast EV-encapsulated drugs could be used in vivo to inhibit osteoclast activity, we induced an acute osteoclast overactivation by administration of retinoid acid[31] and treated the mice once, at day 1 of the experiment, with the free drugs or with EVs isolated from the conditioned media of osteoblasts, collected from one 125-cm^2 flask/mouse (2.5×10^6 osteoblasts/cm^2) and loaded with vehicle, zoledronate, or dasatinib. After 4 days, mice were euthanized, tibias were histochemically stained for TRAcP and evaluated histomorphometrically for the osteoclast variables. As expected, mice receiving retinoic acid underwent a significant reduction of body weight (Fig. 9*A*), indicating the efficacy of the treatment.[31,32] They also showed an increase of the bone resorption marker, collagen type 1 C-telopeptide (CTX) (Fig. 9*B*), and of the osteoclast number (Fig. 9*C*,*D*) and surface (Fig. 9*D*) over bone surface. The increase of these variables was efficiently counteracted by treatment with free zoledronate or dasatinib, while EVs alone had no effect. Remarkably, osteoblast EV-encapsulated drugs reduced osteoclast overactivation (Fig. 9*A*–*E*) and, in the case of EV-Zol, induced apoptosis (Fig. 9*F*,*G*).

Discussion

The involvement of EVs in the communication between bone cells is very poorly understood. Authors have reported vesicle-like structures arising from osteocytes,[39] but with no data on their composition and function. Some EV protein characterization has been reported for osteoblast cell lines,[28,40] and "malignant" osteosarcoma cell EVs have been described to transport osteoclastogenic instruction.[41] Despite these reports, no functional data are available to understand the function of EVs in bone biology.

In our study, we used primary murine osteoblasts and assessed their release of EVs into the environment. We noted in vitro that osteoblasts shuttled lipophilic dyes to distant cells through transwell membranes with porosity up to 1 μm. These results are consistent with the shuttle of EVs from donor cells to distant recipient cells. We confirmed the involvement of EVs in this process, isolating EVs from the conditioned media of osteoblasts, and showing their ability to directly uptake, activate, and retain cytoplasmic dyes, such as CMFDA. These results highlighted that our vesicular structures were cell-derived and that they showed integrity, as shown by the presence of CD63 and by the TEM analysis. These EVs were able to integrate into target cells, including osteoblasts, monocytes, osteoclasts, and endothelial cells, presumably transferring their cargoes. Confocal microscopy analysis showed different patterns of dye accumulation in target cells, suggesting that the integration of EV components is a dynamic and specific process. Different localization of dyes, with or without colocalization in different cell compartments, suggested that EV constituents are recycled in their target cells, likely in a programmed and regulated way, according to their needs.

It has been reported that EVs can exert their effect by ligand/receptor interaction.[16,17,27] Here we found evidence that in bone this type of intercellular communication includes the Rankl/Rank axis. In fact, FACS analysis showed that osteoblast-derived EVs contain Rankl on their surface. Previous reports have shown Rankl presence on EVs from the stromal/osteoblast cell lines UAMS-32P and SV-HFO.[27,28] Although these cells are

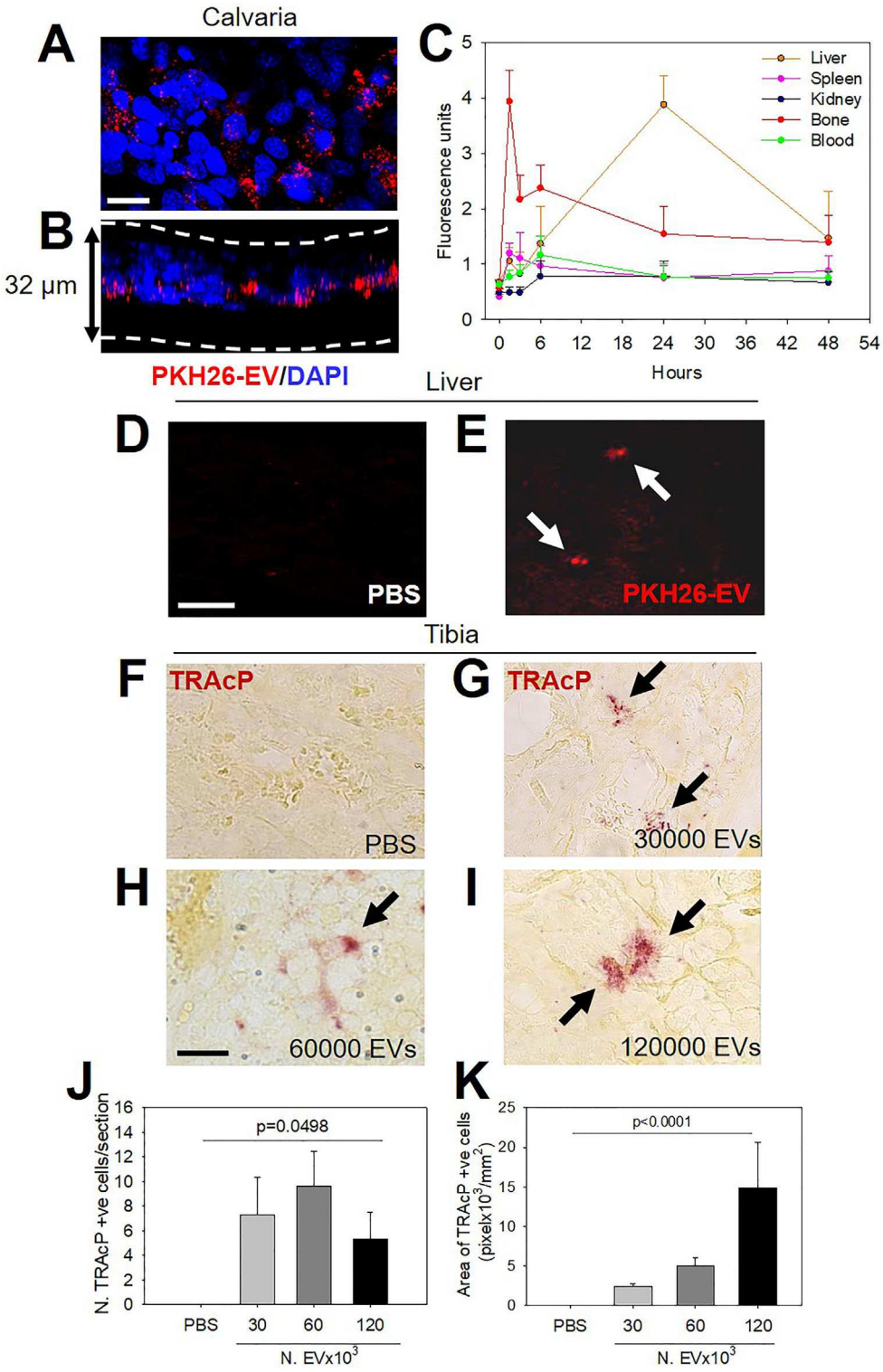

Fig. 8. Osteoblast EV integration, targeting, and biologic activity in bone. (*A*) Confocal microscopy of murine calvaria incubated for 48 hours with PKH26-labeled osteoblast EVs (red). Planar acquisition. (*B*) *z*-Axis scan inside 32 µm. Blue, nuclei stained with Hoechst. Scale bar = 5 µm. (*C*) Time-dependent fluorimetric quantification of PKH26 in the indicated organs from 5-day-old CD1 mice injected intraperitoneally with 30,000 FACS sorted, PKH26-labeled, Rankl-positive osteoblast EVs/mouse. $n = 6$ mice/group. (*D*,*E*) Histological evaluation by confocal microscopy of PHK26 red fluorescence (arrows) in the liver of mice injected with (*D*) vehicle (PBS) or (*E*) PKH26-labeled osteoblast EVs after 24 hours from injection. Scale bar = 5 µm. (*F*–*K*) Histochemical evaluation of proximal tibia sections from 5-day-old *Rankl*$^{-/-}$ mice treated 5 times, every other day, with (*F*) vehicle (PBS) or (*G*) 30,000, (*H*) 60,000, or (*I*) 120,000 RANKL-positive osteoblast EVs/mouse. Sections were histochemically stained for the osteoclast-specific marker, TRAcP. Arrows, TRAcP-positive cells. Quantification of TRAcP-positive cell (*J*) number and (*K*) area. Results are representative (*A*,*B*,*D*–*I*) or the mean ± SD (*C*,*J*,*K*) of three to six mice/group (one-way ANOVA).

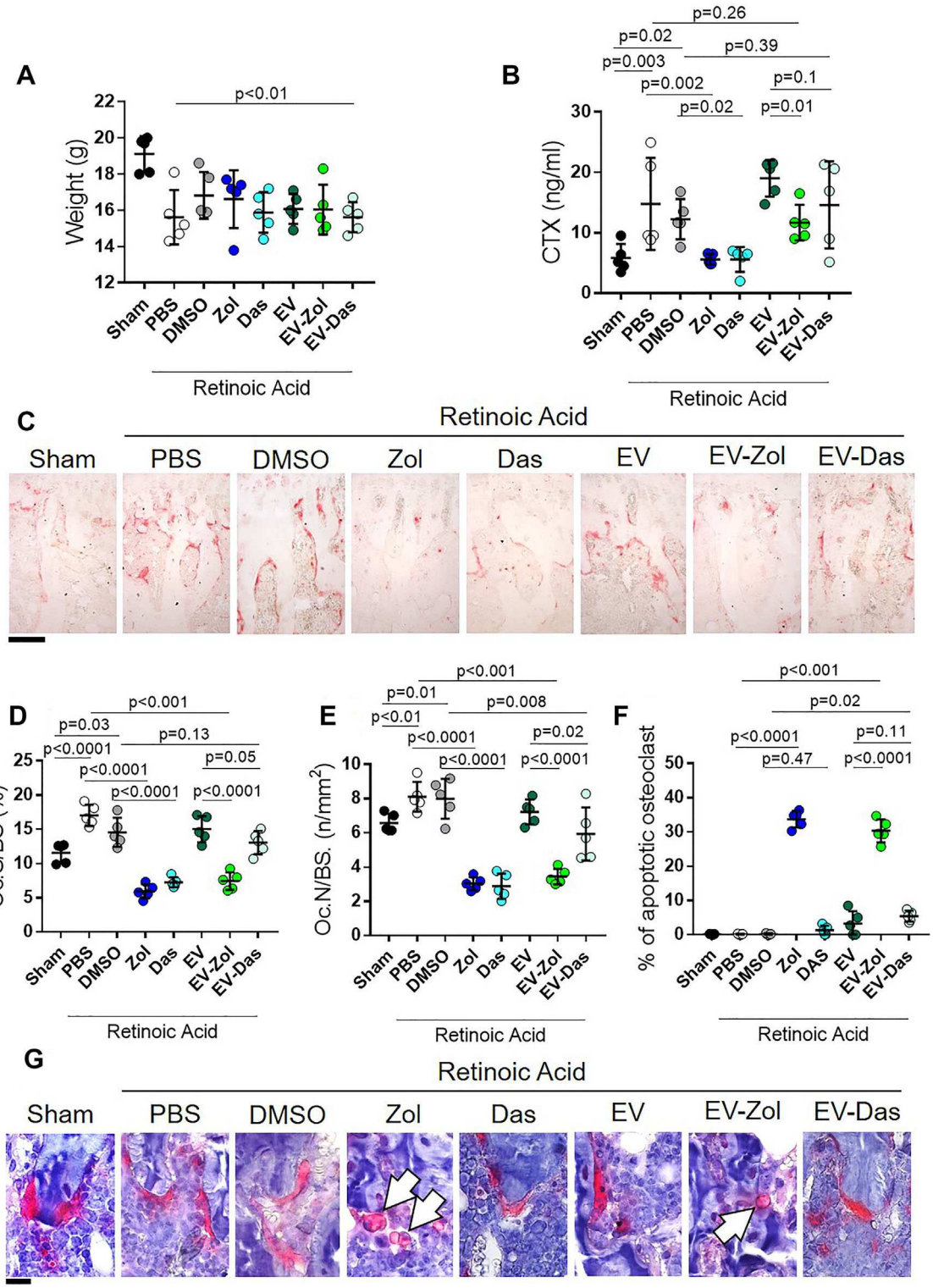

Fig. 9. In vivo effect of osteoblast EV-encapsulated sodium zoledronate and dasatinib on osteoclasts. Eight-week-old C57BL/6J female mice were treated by oral gavage with corn oil (Sham) or with 120 mg/kg bw retinoic acid in corn oil to induce osteoclast overactivation. Retinoic acid-treated mice where then injected i.p. with vehicles (PBS or DMSO), 70 μg/kg bw of Zol, 12.5 mg/kg bw of Das, osteoblast EVs (EVs), or osteoblast EVs loaded with 14 mM sodium zoledronate (EV-Zol) or with 10 mM dasatinib (EV-Das). After 4 days mice were (*A*) weighed, then they were euthanized and blood samples were collected for (*B*) serum CTX quantification. (*C*) Proximal tibia sections were histochemically stained for the activity of the osteoclast-specific enzyme, TRAcP (purple stain). Scale bar = 100 μm. (*D*) Histomorphometric evaluation of Oc.N/BS, (*E*) Oc.S/BS, and (*F*) apoptotic osteoclasts (%). (*G*) High magnification of tibia sections stained for TRAcP (purple) and counterstained with hematoxylin. Arrows: apoptotic osteoclasts. Scale bar = 40 μm. Results are representative (*C*,*G*) or the mean ± SD (*A*,*B*,*D*,*E*,*F*) of five mice per group (unpaired Student's *t* test). Oc.N/BS = osteoclast number/bone surface; Oc.S/BS = osteoclast surface/bone surface; Zol = sodium zoledronate; Das = dasatinib.

established osteoblast-like lines, we believe that they cannot totally mirror the physiology of primary osteoblasts due to acquired genetic aberrations, being similar to tumor cells or viral-gene manipulated cells.[27]

We found Rankl on osteoblast-derived EVs in basal conditions, and this expression was upregulated by PTH. Our results showed that Rankl-positive EVs affected osteoclast function in vitro, increasing their size and number of nuclei. Moreover, the TRAcP staining appeared more intense in EV-treated osteoclasts, suggesting more metabolically active cells. The effect seems to be Rankl-dependent, because *rankl*$^{-/-}$ EVs did not preserve osteoclast vitality, although the rate of EV retrieval was similar in wild-type and *rankl*$^{-/-}$ osteoblasts. Many osteoclasts showed signs of sufferance under *rankl*$^{-/-}$ EV treatment, with cellular retraction and loss of nuclei. These data are consistent with the deprivation of the well-known osteoclast pro-survival function of Rankl.[42] Interestingly, osteoblast EVs appear also to affect the expression of osteoblast-specific genes, suggesting selective autocrine regulation of osteoblast gene expression by means of their own EVs.

A key evaluation of the effect on the osteoclast lineage was represented by the in vivo administration of wild-type osteoblast EVs in *rankl*$^{-/-}$ mice. The *rankl*$^{-/-}$ mouse is a model of human osteoclast-poor autosomal recessive osteopetrosis.[26] Like its human counterpart, this mouse model is characterized by the absence of the osteoclast lineage, and their bones are totally TRAcP-negative. We found an EV density-dependent appearance of TRAcP-positive cells in tibias of *rankl*$^{-/-}$ mice treated with escalating numbers of our EVs, suggesting a biologic effect of the EV-shuttled Rankl. Ex vivo tissue-specific integration experiments in calvariae confirmed the ability of EVs to integrate into the bone cells and in vivo distribution experiments established that osteoblast-derived EVs are preferentially taken up very rapidly by the bone, further suggesting a tissue targeting specificity of the EVs released by osteoblasts.

EVs are known to contain and shuttle RNAs. Many reports over recent years have described the molecular content of EVs isolated from different cells, tissues, and biologic samples.[35] Web compendia about these data, such as ExoCarta (http://exocarta.org/) and Vesiclepedia (http://microvesicles.org/), display growing reporting lists of lipids, RNAs and proteins recognized in various classes of EVs.

To the best of our knowledge, no studies to date have investigated the mRNA profile of EVs from bona fide primary osteoblasts. Here we found that our EVs contain a set of transcripts related to osteoblast activity. Although we are aware that our analysis is limited only to a very partial gene panel and does not measure the absolute quantity of transcripts, we believe that these results could have important biologic relevance. The 15 most abundant mRNAs in osteoblast EVs comprise a set of genes clearly associated with bone metabolism and osteoblast function. *Col1a1* (ID: 12842) encodes the alpha-1 subunit of type I collagen, the most abundant extracellular matrix protein, mainly contained in bone, skin, and tendon.[43] *Col1a2* (ID: 12843) encodes the alpha-2 subunit of the same type I collagen and, in association with the alpha-1 subunit, forms heterotrimeric type I procollagen for fibril formation.[44] *Bglap* (ID: 12096) encodes osteocalcin, one of the most abundant noncollagenous proteins in the mineralized matrix of bone.[44] Osteocalcin is known to exert endocrine activities, regulating energy metabolism, neural development, male fertility, and muscle function.[45–47] Our observation that osteocalcin transcriptional expression is modulated in osteoblasts by their own EVs suggest that EVs could also contribute to the control of the osteoblast endocrine function. *Sparc* (ID: 20692) encodes for the secreted acidic cysteine-rich glycoprotein, or osteonectin, that in bone is involved mainly in the interaction between mineral crystals and collagen, probably triggering the nucleation of hydroxyapatite.[48] Secreted phosphoprotein 1, or osteopontin, is the product of the *spp1* gene (ID: 20750). It plays a role as an integral part of the mineralized matrix and is involved in important cell-matrix interactions.[49] In fact, it has been reported that osteopontin works as a "bridge" between extracellular matrix and cells, acting as a ligand of integrin heterodimers, such as $\alpha v\beta 3$ or $\alpha v\beta 5$,[50–53] and driving osteoblast differentiation.[54] A set of four transcripts are from structural and housekeeping genes, such as *Gapdh* (ID: 14433, glyceraldehyde-3-phosphate dehydrogenase), *Actb* (ID: 11461, actin beta), *B2m* (ID: 12010, β-2 microglobulin) and *Hsp90ab1* (ID: 15516, heat shock protein 90 alpha [cytosolic] class B member 1). A further comparison between EV and cellular transcriptomes did not reveal any preferential sorting or enrichment of mRNAs in EVs; therefore, the osteoblast EVs seem to mirror the transcript profile of their donor cells. This is at variance with what has been described in other cells, in which selective sorting of molecules into EVs was observed.[36]

Due to their ability to shuttle specific cargoes and because of their targeted uptake in tissues, EVs are under intense investigation for various clinical applications. They could be used as "biomarkers" for diagnostic purposes, because they can reflect the molecular content of the donor tissues and are released into the circulation. Therefore, they could be useful in "liquid biopsies" to monitor the progression of diseases or scrutinize the success of therapies.[1,5] Furthermore, they can be loaded with tracking molecules and drugs, widening the therapeutic index, narrowing the median effective dose (ED_{50}) of drugs and reducing the risk of side effects because of their targeted delivery.[8] Here, we showed that osteoblast-derived EVs can be loaded with anti-osteoclastic agents. In particular, we loaded osteoblast-derived EVs with dasatinib, a clinically approved inhibitor of tyrosine kinases for malignancies,[55–59] or with zoledronate, a bisphosphonate clinically approved for osteoporosis.[60–62] Both agents are known to be very effective against osteoclasts. When encapsulated in EVs, both dasatinib and zoledronate still exerted their biologic effects. Das-EVs induced massive retraction and collapse of cells due to the inhibition of crucial tyrosine kinases, such as c-Src, involved in osteoclast cytoskeletal remodeling and actin ring formation.[31,63] Zol-EVs induced vacuolization and apoptosis of osteoclasts, consistent with inhibition of the mevalonate and lipid pathways known to be disrupted by N-bisphosphonates.[64,65] The EV-encapsulated drugs maintained their efficacy, as shown by the degeneration of osteoclasts similar to that induced by the free drugs. Most importantly, this anti-osteoclastic activity was observed also in vivo in an acute mouse model of osteoclast over-activation, thus supporting their in vivo use to shuttle pharmacological agents to bone cells.

The proof of principle that EVs can have a potential therapeutic effect in bone pathology was further uncovered by our in vivo results in Rankl-deficient mice. Mice harboring mutations in the *tnsf11a* gene are the genocopy/phenocopy of human autosomal recessive osteopetrosis 2 (OMIM: #259710, OPTB2).[26] Presently, the patients are untreatable, have a very poor quality of life and a short life expectancy. They could take advantage of substitutive therapy with soluble Rankl,[66] but a pharmacological formulation of Rankl is not under

development. On this basis, the hypothesis of the use of clinical-grade EVs from healthy donors or engineered from patient cells to carry the wild-type protein, could help setting a new strategy for treating, or at least alleviating the symptoms, of this lethal disease. More widely, we can image EVs as a shuttle for delivery of membrane-bound molecules, cytokines, and growth factors like the Rankl reported in this study.

In conclusion, this report demonstrates that osteoblast EVs play a physiologic role in the interaction with other cells in the bone microenvironment, especially monocytes and osteoclasts. Moreover, we reported a proof of concept for the use of osteoblast-derived EVs for the treatment of bone diseases, because they are able to efficiently target the bone and induce clear biologic events, both by endogenous (Rankl) and exogenous (bisphosphonates and tyrosine kinase inhibitors) molecules, opening an avenue for their biotechnological use to treat skeletal disorders.

Disclosures

All Authors declare no conflict of interest.

Acknowledgments

This work was supported by an Investigator Award from the "Società Italiana di Osteoporosi, del Metabolismo Minerale e delle Malattie dello Scheletro" to AC, by grants from the "Ricerca Corrente" of the Ospedale Pediatrico Bambino Gesù to MM, by a grant of the "Associazione Italiana per la Ricerca sul Cancro" to NR, by the European Commission grant Program "Collaborative Project – Large-scale integrating project" – Call identifier: FP7-HEALTH.2012.2.1.1-1-C Proposal No 602300 – Acronym: SYBIL to AT.

Authors' roles: Study design: AC, MM, and AT. Study conduct: AC, AL, and AM. Data collection: AC, AM, NR, and AT. Data analysis: AC, AL, AM, NR, and AT. Data interpretation: AC, AL, NR, MM, and AT. Drafting manuscript: AC, AL, and AT. Revising manuscript content: AC, AL, MM, AM, NR, and AT. Approving final version of manuscript: AC, AL, MM, AM, NR, and AT.

References

1. Yáñez-Mó M, Siljander PR, Andreu Z, et al. Biological properties of extracellular vesicles and their physiological functions. J Extracell Vesicles. 2015;4:27066.
2. Cocucci E, Meldolesi J. Ectosomes and exosomes: shedding the confusion between extracellular vesicles. Trends Cell Biol. 2015;25:364–72.
3. Raposo G, Stoorvogel W. Extracellular vesicles: exosomes, microvesicles, and friends. J Cell Biol. 2013;200:373–83.
4. Kim DK, Lee J, Kim SR, et al. EVpedia: a community web portal for extracellular vesicles research. Bioinformatics. 2015;1:933–9.
5. Lo Cicero A, Stahl PD, Raposo G. Extracellular vesicles shuffling intercellular messages: for good or for bad. Curr Opin Cell Biol. 2015;35:69–77.
6. Gho YS, Lee C. Emergent properties of extracellular vesicles: a holistic approach to decode the complexity of intercellular communication networks. Mol Biosyst. 2017;13:1291–96.
7. Colombo M, Raposo G, Théry C. Biogenesis, secretion, and intercellular interactions of exosomes and other extracellular vesicles. Ann Rev Cell Dev Biol. 2014;30:255–89.
8. El Andaloussi S, Mäger I, Breakefield XO, Wood MJ. Extracellular vesicles: biology and emerging therapeutic opportunities. Nat Rev Drug Discov. 2013;12:347–57.
9. Pitt JM, Kroemer G, Zitvogel L. Extracellular vesicles: masters of intercellular communication and potential clinical interventions. J Clin Invest. 2016;126:1139–43.
10. Quesenberry PJ, Aliotta J, Deregibus MC, Camussi G. Role of extracellular RNA-carrying vesicles in cell differentiation and reprogramming. Stem Cell Res Ther. 2015;6:153.
11. Kholia S, Ranghino A, Garnieri P, et al. Extracellular vesicles as new players in angiogenesis. Vascul Pharmacol. 2016;86:64–70.
12. Collino F, Pomatto M, Bruno S, et al. Exosome and microvesicle-enriched fractions isolated from mesenchymal stem cells by gradient separation showed different molecular signatures and functions on renal tubular epithelial cells. Stem Cell Rev. 2017;13:226–43.
13. Chen T, Guo J, Yang M, Zhu X, Cao X. Chemokine-containing exosomes are released from heat-stressed tumor cells via lipid raft-dependent pathway and act as efficient tumor vaccine. J Immunol. 2011;186:2219–28.
14. Colombo M, Moita C, van Niel G, et al. Analysis of ESCRT functions in exosome biogenesis, composition and secretion highlights the heterogeneity of extracellular vesicles. J Cell Sci. 2013;126:5553–65.
15. Johnsen KB, Gudbergsson JM, Skov MN, Pilgaard L, Moos T, Duroux M. A comprehensive overview of exosomes as drug delivery vehicles—endogenous nanocarriers for targeted cancer therapy. Biochim Biophys Acta. 2014;1846:75–87.
16. Rivoltini L, Chiodoni C, Squarcina P, et al. TNF-Related Apoptosis-Inducing Ligand (TRAIL)-armed exosomes deliver proapoptotic signals to tumor site. Clin Cancer Res. 2016;22:3499–512.
17. Sidhu SS, Mengistab AT, Tauscher AN, LaVail J, Basbaum C. The microvesicle as a vehicle for EMMPRIN in tumor-stromal interactions. Oncogene. 2004;23:956–63.
18. Hoshino A, Costa-Silva B, Shen TL, et al. Tumour exosome integrins determine organotropic metastasis. Nature. 2015;527:329–35.
19. Luga V, Zhang L, Viloria-Petit AM, et al. Exosomes mediate stromal mobilization of autocrine Wnt-PCP signaling in breast cancer cell migration. Cell. 2012;151:1542–56.
20. Kim J, Shin H, Park J. RNA in salivary extracellular vesicles as a possible tool for systemic disease diagnosis. J Dent Res. 2017;96:938–44
21. Chandler WL. Measurement of microvesicle levels in human blood using flow cytometry. Cytometry B Clin Cytom. 2016;90:326–36.
22. Choi M, Ban T, Rhim T. Therapeutic use of stem cell transplantation for cell replacement or cytoprotective effect of microvesicle released from mesenchymal stem cell. Mol Cell. 2014;37:133–9.
23. Cappariello A, Ponzetti M, Rucci N. The "soft" side of the bone: unveiling its endocrine functions. Horm Mol Biol Clin Investig. 2016;28:5–20.
24. Simonet WS, Lacey DL, Dunstan CR, et al. Osteoprotegerin: a novel secreted protein involved in the regulation of bone density. Cell. 1997;89:309–19.
25. Kong YY, Yoshida H, Sarosi I, et al. OPGL is a key regulator of osteoclastogenesis, lymphocyte development and lymph-node organogenesis. Nature. 1999;397:315–23.
26. Sobacchi C, Schulz A, Coxon FP, Villa A, Helfrich MH. Osteopetrosis: genetics, treatment and new insights into osteoclast function. Nat Rev Endocrinol. 2013;9:522–36.
27. Deng L, Wang Y, Peng Y, et al. Osteoblast-derived microvesicles: a novel mechanism for communication between osteoblasts and osteoclasts. Bone. 2015;79:37–42.
28. Morhayim J, van de Peppel J, Demmers JAA, et al. Proteomic signatures of extracellular vesicles secreted by nonmineralizing and mineralizing human osteoblasts and stimulation of tumor cell growth. FASEB J. 2015;29:274–85.
29. Morhayim J, Rudjito R, van Leeuwen JP, van Driel M. Paracrine signaling by extracellular vesicles via osteoblasts. Curr Mol Biol Rep. 2016;2:48–55.
30. Pierroz DD, Rufo A, Bianchi EN, et al. β-Arrestin2 regulates RANKL and ephrins gene expression in response to bone remodeling in mice. J Bone Miner Res. 2009;24:775–84.

31. Recchia I, Rucci N, Funari A, et al. Reduction of c-Src activity by substituted 5,7-diphenyl-pyrrolo[2,3-d]-pyrimidines induces osteoclast apoptosis in vivo and in vitro. Involvement of ERK1/2 pathway. Bone. 2004;34:65–79.
32. Rucci N, Capulli M, Ventura L, et al. Proline/arginine-rich end leucin-rich repeat protein N-terminus is a novel osteoclast antagonist that counteracts bone loss. J Bone Miner Res. 2013;28:1912–24.
33. Dempster DW, Compston JE, Drezner MK, et al. Standardized nomenclature, symbols and units for bone histomorphometry: a 2012 update of the report of the ASBMR Histomorphometry Nomenclature Committee. J Bone Miner Res. 2013;28:2–17.
34. Akuthota P, Carmo LA, Bonjour K, et al. Extracellular microvesicle production by human eosinophils activated by "inflammatory" stimuli. Front Cell Dev Biol. 2016;4:117.
35. Iraci N, Leonardi T, Gessler F, Vega B, Pluchino S. Focus on extracellular vesicles: physiological role and signalling properties of extracellular membrane vesicles. Int J Mol Sci. 2016;17:171.
36. Zomer A, Vendrig T, Hopmans ES, van Eijndhoven M, Middeldorp JM, Pegtel DM. Exosomes: fit to deliver small RNA. Commun Integr Biol. 2010;3:447–50.
37. Wiklander OP, Nordin JZ, O'Loughlin A, et al. Extracellular vesicles in vivo biodistribution is determined by cell source, route of administration and targeting. J Extracell Vesicles. 2015;4:26316.
38. Haga H, Yan IK, Takahashi K, Matsuda A, Patel T. Extracellular vesicles from bone marrow-derived mesenchymal stem cells improve survival from lethal hepatic failure in mice. Stem Cells Transl Med. 2017;6:1262–72.
39. Kamel-ElSayed SA, Tiede-Lewis LM, Lu Y, Veno PA, Dallas SL. Novel approaches for two and three dimensional multiplexed imaging of osteocytes. Bone. 2015;76:129–40.
40. Nair R, Santos L, Awasthi S, et al. Extracellular vesicles derived from preosteoblasts influence embryonic stem cell differentiation. Stem Cells Dev. 2014;23:1625–35.
41. Garimella R, Washington L, Isaacson J, et al. Extracellular membrane vesicles derived from 143B osteosarcoma cells contain pro-osteoclastogenic cargo: a novel communication mechanism in osteosarcoma bone microenvironment. Transl Oncol. 2014;7:331–40.
42. Luo J, Yang Z, Ma Y, et al. LGR4 is a receptor for RANKL and negatively regulates osteoclast differentiation and bone resorption. Nat Med. 2016;22:539–46.
43. Shoulders MD, Raines RT. Collagen structure and stability. Ann Rev Biochem. 2010;78:929–58.
44. Komori T. Regulation of bone development and extracellular matrix protein genes by RUNX2. Cell Tissue Res. 2010;339:189–95.
45. Karsenty G, Oury F. Regulation of male fertility by the bone-derived hormone osteocalcin. Mol Cell Endocrinol. 2014;382:521–6.
46. Li J, Zhang H, Yang C, Li Y, Dai Z. An overview of osteocalcin progress. J Bone Miner Metab. 2016;34:367–79.
47. Mera P, Laue K, Ferron M, et al. Osteocalcin signaling in myofibers is necessary and sufficient for optimum adaptation to exercise. Cell Metab. 2016;23:1078–92.
48. Rosset EM, Bradshaw AD. SPARC/osteonectin in mineralized tissue. Matrix Biol. 2016;52–54:78–87.
49. Bouleftour W, Juignet L, Bouet G, et al. The role of the SIBLING, bone sialoprotein in skeletal biology—contribution of mouse experimental genetics. Matrix Biol. 2016;52–54:60–77.
50. Owen RM, Carlson CB, Xu J, Mowery P, Fasella E, Kiessling LL. Bifunctional ligands that target cells displaying the αvβ3 integrin. Chem Biochem. 2007;8:68–82.
51. Hu DD, Lin EC, Kovach NL, Hoyer JR, Smith JW. A biochemical characterization of the binding of osteopontin to integrins alpha v beta 1 and alpha v beta 5. J Biol Chem. 1995;270:26232–8.
52. Yokosaki Y, Tanaka K, Higashikawa F, Yamashita K, Eboshida A. Distinct structural requirements for binding of the integrins alphavbeta6, alphavbeta3, alphavbeta5, alpha5beta1 and alpha9-beta1 to osteopontin. Matrix Biol. 2005;24:418–27.
53. Liaw L, Skinner MP, Raines EW, et al. The adhesive and migratory effects of osteopontin are mediated via distinct cell surface integrins: role of αvβ3 in smooth muscle cell migration to osteopontin in vitro. J Clin Invest. 1995;95:713–24.
54. Huang W, Carlsen B, Rudkin G, et al. Osteopontin is a negative regulator of proliferation and differentiation in MC3T3-E1 pre-osteoblastic cells. Bone. 2004;34:799–808.
55. Talpaz M, Shah NP, Kantarjian H, et al. Dasatinib in imatinib-resistant Philadelphia chromosome-positive leukemias. N Engl J Med. 2006;354:2531–41.
56. Araujo J, Logothetis C. Dasatinib: a potent SRC inhibitor in clinical development for the treatment of solid tumors. Cancer Treat Rev. 2010;36:492–500.
57. Pichot CS, Hartig SM, Xia L, et al. Dasatinib synergizes with doxorubicin to block growth, migration, and invasion of breast cancer cells. Br J Cancer. 2009;101:38–47.
58. Finn RS, Dering J, Ginther C, et al. Dasatinib, an orally active small molecule inhibitor of both the src and abl kinases, selectively inhibits growth of basal-type/"triple-negative" breast cancer cell lines growing in vitro. Breast Cancer Res Treat. 2007;105:319–26.
59. Copland M, Hamilton A, Elrick LJ, et al. Dasatinib (BMS-354825) targets an earlier progenitor population than imatinib in primary CML but does not eliminate the quiescent fraction. Blood. 2006;107:4532–39.
60. Grey A. Intravenous zoledronate for osteoporosis: less might be more. Ther Adv Musculoskelet Dis. 2016;8:119–23.
61. Bolland MJ, Grey AB, Horne AM, et al. Effects of intravenous zoledronate on bone turnover and bone density persist for at least 24 months. J Bone Miner Res. 2008;23:1304–8.
62. Doggrell SA. Zoledronate once-yearly increases bone mineral density—implications for osteoporosis. Expert Opin Pharmacother. 2002;3:1007–9.
63. Teti A, Taranta A, Migliaccio S, et al. Colony stimulating factor-1-induced osteoclast spreading depends on substrate and requires the vitronectin receptor and the c-src proto-oncogene. J Bone Miner Res. 1998;13:50–8.
64. Russell RGG. Bisphosphonates: from bench to bedside. Ann N Y Acad Sci. 2006;1068:367–401.
65. Breuer E. The development of bisphosphonates as drugs. In: Fischer J, Ganellin CR, editors. Analogue-based drug discovery. Weinheim, Germany: Wiley-VCH Verlag GmbH & Co. KGaA; 2006. p. 371–84.
66. Lo Iacono N, Blair HC, Poliani PL, et al. Osteopetrosis rescue upon RANKL administration to Rankl(–/–) mice: a new therapy for human RANKL-dependent ARO. J Bone Miner Res. 2012;27:2501–10.